Modeling the baroreflex : development of a blood pressure control model as a tool for baroreflex sensitivity analysis

Pellis, B.J.

Award date:
1998

TNO Institute of Applied Physics
Biomedical Instrumentation

University of Technology Eindhoven

Modeling the Baroreflex

Development of a blood pressure control model as
a tool for baroreflex sensitivity analysis

By B.J. Pellis

Written by order of	:	Prof. dr. ir. P.P.J. van den Bosch *Chairman of department MBS TU Eindhoven*
		Dr. ir. J.A. Blom *Chairman of department MBS section EME TU Eindhoven*
Supervisor	:	Prof. ir. K.H. Wesseling *Professor at department MBS section EME TU Eindhoven / TNO BMI Amsterdam*
Coach	:	Ir. J.J. Settels *TNO BMI Amsterdam*

Summary

The human blood pressure control system is a complex system that is controlled by many regulating mechanisms. For many years investigators have gathered insight in the system. Simulation models has proved to be valuable in understanding these mechanisms. Though until now, some aspects are still not clear. Recently baroreflex sensitivity analysis is under discussion. In this thesis we developed a model that can be used to gather insight in these obscurities.

The model consist of a circulation model and a control model. In the circulation model we approached all parts of the vessels as elastic tubes, which corresponds with the physiology. For most parts of the circulation a linear elastance. For the aorta we used a nonlinear model and in the ventricles we used a time-varying elastance. The pulmonary circulation is approached similar to the systemic circulation with all linear elements. Yet, we realize that this is a simplification towards the real physiology, for our aim it meets the requirements.

In the control model we focused on the baroreflex being the most important of all regulating mechanisms in short time analysis. Baroreceptors are designed as a nonlinear transfer. The effectors of the system are both vagal as sympathetic heart rate control, peripheral resistance, venous volume and contractility control. All these effectors are approached as a lowpass filter containing a time delay, time constant, gain and offset.

To test our model behavior we performed several experiments. Besides looking at signals at free run experiments we also looked at open and closed loop gains of the system. The outcomes of these experiments agrees with former studies and with measurements done in humans. Furthermore we looked at blood pressure and heart rate variability. By introducing noise sources in our model we generate these blood pressure and heart rate variability. Looking at the estimated spectra we concluded that these spectra reasonable mimics measured spectra.

Preface

This paper is the report of my work in partial fulfillment of the requirements for the ir-degree at the Eindhoven University of Technology, faculty of Electrical Engineering. The work is performed at the TNO Institute of Applied Physics, department of Biomedical Instrumentation (BMI). TNO offered me the possibility to do a research at their department in Amsterdam, for which I want to thank the management of TNO BMI.

I want to thank dr. ir. P.J.M. Cluitmans of the Eindhoven University of Technology for bringing me into contact with TNO.

Especially I want to thank prof. ir.K.H. Wesseling for his coaching, assistance, critical remarks and discussion during the project, and not in the least during the genesis of this report.

Thanks to ir. J.J. Settels for his coaching and for the involvement he showed to make this assignment successful.

Furthermore I want to thank all my colleagues at the BMI institute who made my stay rememberable thanks to the pleasant cooperation and working atmosphere.

Finally I want to thank prof. dr. ir. P.P.J. van den Bosch and dr. ir. J.A. Blom who took the final responsibility for my assignment.

Contents

Chapter 1 General

1.1 Introduction

The human cardiovascular system consists of a large number of blood vessels that pervade the whole human body and that is driven by the heart. Its main purposes are:

- to supply oxygen to the tissues
- to remove carbon dioxide
- to distribute nutrients
- to regulate heat

In importance the last three are inferior to oxygen supply. Although the organs and tissues can survive a lack of nutrition for quite some time, a shortage of oxygen will be fatal within several minutes. To provide a sufficient blood supply in all parts of the human body, the circulation is tightly controlled. Control actions with various time constants regulate the blood circulation in the short term (seconds to hours) and the long term (days to years).

The study of the circulation and its many control loops has been under long investigation and has led to a systems approach of the circulation. Each of the various subsystems is described in the form of mathematical formulae and constitutive equations, the complete set of which serves as a model of the circulation. Many different models exist. Most approaches are similar, but have different points of view on some parts. Ten Voorden [15] reviews some of the models that can be seen as roots on which others are based.

One of the earlier computer models of the circulation was developed at TNO and published in 1967 [2]. An analog computer was used to describe pressure, flow and volume relations. A simple baroreflex control mechanism was included. Now, 30 years later, investigators have gathered more insight in most parts of the circulation. The availability of fast digital computers and introduction of the non-invasive finger arterial blood pressure monitor Finapres (allowing detailed studies of continuous blood pressure measurements) has contributed to detailed models of the circulation with its control loops. There are, however, many areas still under discussion.

Recent studies are focusing on analyzing the condition of the blood pressure control of people. Older people or people with cardiovascular diseases can have conditions in which blood pressure control fails. In these cases, doctors want to localize the point of failure and indicate its degree. Recent publications have described methods to judge the condition of the blood pressure control system,

especially the fastest control mechanism, the baroreflex. Circulatory challenges causing the control mechanisms to go out of equilibrium and the responses to these challenges are studied. There are many different challenges and protocols used, ranging from drug infusions to non-invasive manoeuver, in order to estimate baroreflex sensitivity. The values as obtained by different stimuli can differ in time and between patients. The model that we will describe in the following sections is can be used to investigate these baroreflex sensitivity experiments.

1.2 Objectives of the model study

This paper is the report of my work in partial fulfillment of the requirements for the ir-degree at the Eindhoven University of Technology. The work is performed at the TNO Institute of Applied Physics, department of Biomedical Instrumentation (BMI). To investigate the properties of the baroreflex, a model describing the short-term blood pressure control system was developed. Our main objective is to gather insight in how a model can be suited to be useful for baroreflex sensitivity studies.

Earlier models at BMI proved to be valuable tools for studying the baroreflex. Our objective now is to *further develop and detail the model*, so that it can be used to investigate challenge responses and to study and understand baroreflex sensitivity measurements.

As the earlier model was written in Pascal code the mathematics are difficult to unravel and adjustments to the model are difficult to implement. We have chosen therefore to convert the model implementation to the simulation program Simulink of the Mathworks company. This simulation program is visually oriented and is running under Windows. There is a direct interface with Matlab, a computing environment also of the Mathworks company. Thus *converting the current model* from Pascal to Simulink is one task.

There is a continuing need to *adjust the model* to recent physiological insights. The model that we use as 'source' for the new model is partially based on outdated information. Better measurement techniques have gathered new insight and led to new concepts. As a second task we want to update the current model to a more modern one.

When we have a Simulink model running, we have to *validate the model* so that the model is reliable and agrees with measurements obtained from the human circulation. To apply the model to studies investigating challenge responses and baroreflex sensitivity, we need some new extensions in the model. As a third task we wanted to *prepare the model* for these studies by implementing needed extensions.

1.3 Outline of this thesis

In chapter 2 we will first describe the blood pressure control system. First we will determine the system structure according control theory. Then we will describe the properties of the cardiovascular system. Further we give a brief overview of all regulating systems. The most important control system, the baroreflex, is described in more detail. The other important mechanisms are briefly described. The performance of the blood pressure control system is reviewed at the end of the chapter.

Chapter 3 handles the circulation model. What is described in the previous chapter is translated to mathematical relation as it is implemented in the model. For the circulation, the concept of elastic tubes that is used in the circulation model is described. Then non-linearity applied to this concept are described. The heart model is described in detail here. The chapter is ended with an overview of the model.

The model of the baroreflex is described in chapter 4. The concept used in the model is described with its mathematical relations. Sensors and processing system are described followed by a description of all effectors. The chapter is ended with an overview of the model.

The model described in chapter 3 and 4 is tested with several experiments. The description and outcome of these experiments are described in chapter 5. First we look at the beat-to-beat variables in the different parts of the circulation. Then we look at the shape of the pressure and flow waveforms. The control system is validated by looking at the loop gains of all effectors in steady-state as well as over the whole spectrum. The concept of baromodulation to explain variation in blood pressure is discussed. The effect of baromodulation on blood pressure and cardiac output is studied. At the end of this chapter we look at a wider time interval and add noise sources to the system in order to simulate the short term variability behavior.

The thesis is finished in chapter 7 with a general discussion. Modeling issues such as parameter estimates and spectral analysis are discussed here.

Chapter 2 Blood pressure control

2.1 Structure

In terms of control theory the blood pressure control system can be seen as a negative feedback control system. A general diagram of such a system is given in figure 2.1 [3].

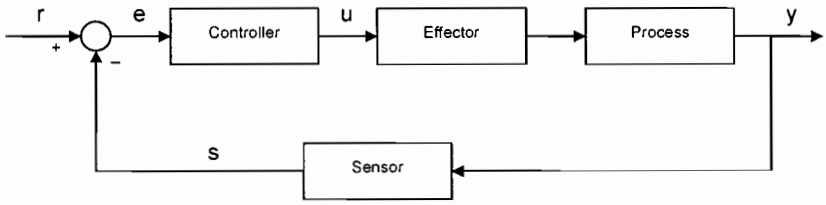

Figure 2.1 *General structure of the control system*

The system regulates the *output value (y)* that is measured by a sensor. Its sensor output (s) is compared with a *set-point (r)* with the aim to minimize the difference between these two signals, the *error signal (e)*. The output of the *process* is regulated by the *controller* by means of its effectors. These *effectors* are the actuators of the controller of the process. In circulation control we can translate these blocks and signals as shown in table 2.1.

Table 2.1 *Blocks and signals from the general feedback system translated to the circulation control.*

General system	Circulation
Process	blood vessels + heart
Controller	Central Nervous System
Effector	e.g. heart rate, peripheral resistance
Sensor	e.g. baroreceptors
Output value (y)	e.g. arterial pressure
Sensor signal (s)	afferent nerve activity
Reference input (r)	set by higher brain centers
Control signal (u)	efferent nerve activity

The general control system of figure 2.1 is an illustration of the structure of the circulation control.

However the real situation is more complicated than this. For example the system of figure 2.1 shows a reference input that is a signal from outside the system. In the human body such a signal may be present in higher brain centers but it has been impossible to locate it.

Furthermore the general system assumes a single input single output (SISO) system while in circulation control multiple inputs and outputs (MIMO) can be found. The output of the system is defined as the input of the sensor. These sensors are based on pressures, so according to the system structure the outputs are pressures. However, pressure is not the only controlled variable in the circulation control. Blood flow is as important as blood pressure. But because in the human body no sensor has been found to measure the flow, this cannot be defined as output in the system structure.

More complexity is present in the blood pressure control system because multiple regulating loops are interacting on the system. We must bear all this in mind looking at the simplified structure of figure 2.1.

Now we will have a closer look at the different subsystems. First we will look at the heart and blood vessels defined as the process. Then we will look at the controller including the effectors and sensors of the system.

2.2 Blood vessels and heart

The circulation consists of a double pulsatile pump (left and right heart), two branching distributing networks of blood vessels (pulmonary and systemic arteries), two branching collecting networks of blood vessels (pulmonary and systemic veins) and a large number of peripheral flow systems. This is illustrated in figure 2.2 [18] in a simplified form.

The right heart pumps blood into the pulmonary circulation, the left heart pumps blood into the systemic circulation. Oxygen is picked up in the lungs and transported to the body by the pulmonary venous and systemic arterial system. Carbon dioxide is picked up in the tissues and transported by the systemic venous system and pulmonary arteries to the lungs where it is exhaled. Nutrition is picked up in the digestive tract and converted and stored in the liver, from where it is released into the systemic venous system in a controlled fashion.

As can be seen in figure 2.2 most organ blood supplies are parallel connected. So reducing the blood flow in one part will not necessarily reduce the blood flow in the other parts. The blood flows from one big artery (aorta) through several parallel connected smaller arteries to a large amount of arterioles and from there to the capillaries which number is estimated as 10^{10}. From here the veins return the blood starting with a large number of small venules to several bigger veins and ending in one major vein (vena cava). From the aorta to the capillaries the total cross sectional area increases 800 fold. The blood flow velocity is reduced proportionally. The total blood volume in human adults is normally about 6 liters, of which the veins contain about 75 percent [12].

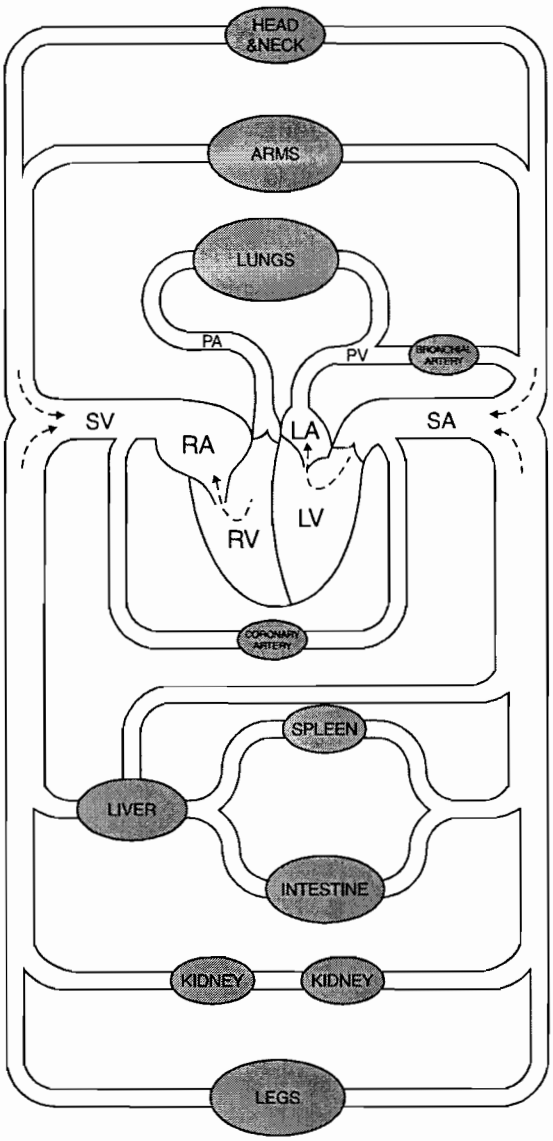

Figure 2.2 *Model of the human circulation (RA = right atrium, RV = right ventricle, PA = pulmonary arteries, PV = pulmonary veins, LA = left atrium, LV = left ventricle, SA = systemic arteries, SV = systemic veins)*

The heart is a pulsatile pump that can be divided in two halves. Each halve is working under different circumstances. In the systemic arteries close to the left ventricle the mean pressure is about 90 mmHg, in the pulmonary artery close to the right ventricle the mean pressure is about 15 mmHg. The flow however must be equal, since they are series connected. Each halve consists of two sub-pumps: the atrium and the ventricle. The left ventricle has a powerful muscle that can develop high pressure in the arteries. The atria help filling the ventricles when these ventricles are relaxed.

To supply the organs and tissues with enough oxygen, is the most critical and therefore the primary design criteria. This means that blood flow must be high enough and distributed over the body according to the corresponding demands of oxygen. To get this blood flow a pressure must be generated depending on the resistance of the blood vessels. If we look at the process, we see that the circulation is (as the word implies) a closed system. This means for example changing resistance in

one part of the body will affect both pressure and flow over the whole system. We can say that the system is always looking for an equilibrium of pressures and flows.

As a result of the rhythmically contracting heart, the pressures in the system will be pulsating. A generalized overview of pressure levels and pulsations is given in figure 2.3 [7].

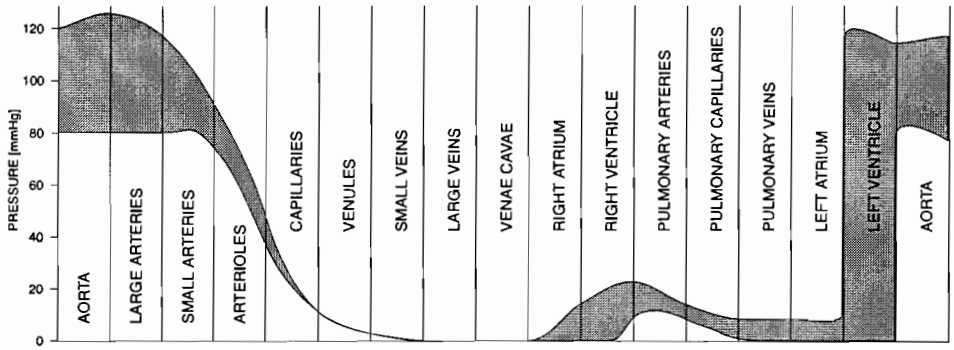

Figure 2.3 *Pressure levels, including oscillatory magnitudes, around the circuit.*

Average circulation time is about 1 minute. The total resting amount of blood pumped by the heart is about 6 l/min, at maximal exercise it is about 25 l/min. The amount of blood pumped by the heart per unit time is called cardiac output. The amount of blood ejected with each cardiac contraction is called the stroke volume.

To get a good blood circulation the mean pressure in the system must be sufficiently high and stable in time. The pulsations of the arterial pressure is kept between an upper and a lower level, called respectively systolic and diastolic pressure. Normal values for the arterial pressures are 120 mmHg systolic, 80 mmHg diastolic and 90 mmHg mean pressure. The control system takes care of this.

2.3 Baroreflex

In figure 2.4 [4] the most important mechanisms controlling blood pressure are illustrated. As shown the fastest controller operating in the normal pressure range (80-150 mmHg) is the baroreflex. Other control mechanisms in the normal blood pressure range are slower, or have a lower gain. Therefore, the baroreflex is the most important control system in short term blood pressure regulation.

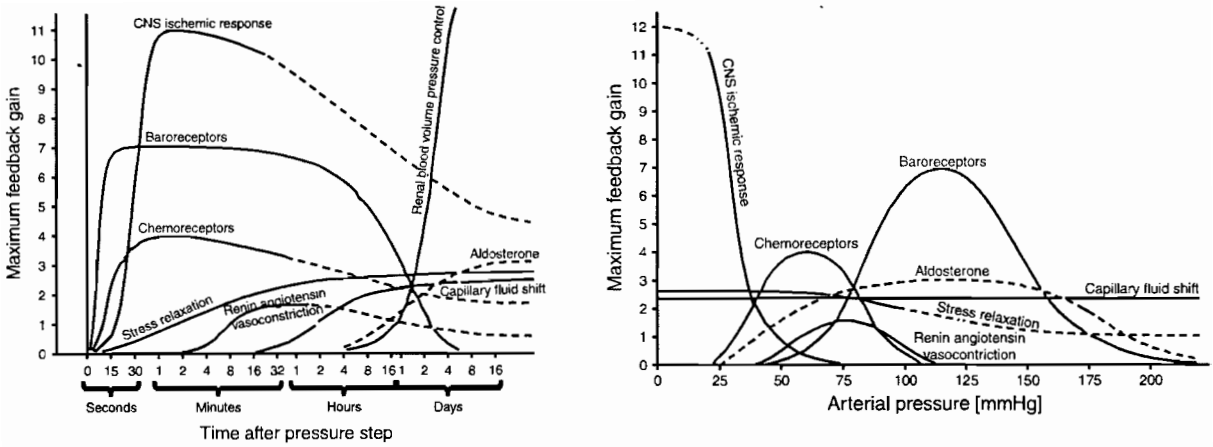

Figure 2.4 *Feedback gain of all blood pressure control mechanisms as function of time (left) and pressure (right)*

The sensors of the baroreflex are the baroreceptors situated in the elastic vessel walls of the aortic arch and the carotid sinus (arteries to the brain). These sensors respond to stretching of the wall by generating impulses in their afferent nerves. High pressure in the vessels causes a higher impulse rate than low pressure. The impulses are conducted to the central nervous system (CNS) in the brain. From here the activation to the effectors in the control loop is changed.

For this study four main effectors are relevant to control blood pressure:

- heart rate
- systemic resistance
- blood volume.
- contractility of the heart

The four effectors are acting on a different time scale and have different effectiveness, this is illustrated in figure 2.5 [20] (contractility of the heart is not shown). The changing of venous volume is the most effective but slowest action. Changing peripheral resistance is faster but less effective and changing heart rate is almost immediate but is even less effective. Contractility of the heart is not shown in figure 2.5 but is the least effective of all four effectors.

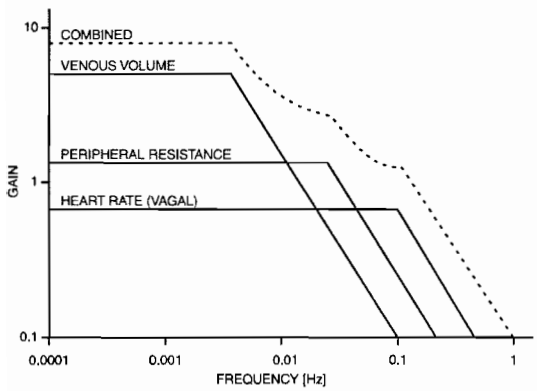

Figure 2.5 *Open loop gain of the three major effectors of the baroreflex*

2.3.1 Baroreflex on heart rate

If we look at the simple equation 2.1 between blood flow (q), heart rate (f_H), and stroke volume (V_S) we can see that an increase of heart rate will result in an increase of blood flow if V_S is constant.

$$q = f_H \, V_S \tag{2.1}$$

There are two nervous path ways in the CNS to effect the heart rate. These are the sympathetic and the parasympathetic nerves (also called vagal nerves). Increasing the vagal frequency will cause a decrease in heart rate while sympathetic frequency increase will cause a heart rate increase. The response to simultaneous activity in the two mechanisms is usually not the algebraic sum of the individual responses. A significant interaction may exist. As the vagal responses are much faster than the sympathetic responses, the vagal response will have immediate effect on the regulation.

2.3.2 Baroreflex on peripheral resistance

The influence of the peripheral resistance will be clear by looking at the simple relation between pressure and resistance. Equation 2.2 shows this relation called Poiseuille's law, with q blood flow, Δp pressure difference between in- and output, η blood viscosity, L length of the vessel, r radius of the vessel and R_s peripheral resistance.

$$q = \frac{\Delta p \, \pi r^4}{L 8 \eta} = \frac{\Delta p}{R_S} \qquad \textit{with:} \qquad R_S = \frac{L 8 \eta}{\pi r^4} \tag{2.2}$$

As we can see an increase of the peripheral resistance will cause an increase of the pressure at equal flow or decrease the flow at equal pressure. In the circulation both affects take place. Also in equation 2.2 can be seen that changing the radius of a vessel will have a great influence on the resistance (4th power). As length and viscosity are constant, resistance changes are strongly dependent on vessel radius. In short the peripheral resistance changes depend on changes in vessel radius of the smaller vessels (arterioles). The process of widening and narrowing vessel radius is also called vaso-dilation and vaso-constriction.

2.3.3 Baroreflex on volume

Another way to influence the blood pressure is by means of the volume. Increasing the vessel volume

will drop the pressure. The veins contains 75 % of the total blood volume. Therefore, changing this volume has the greatest influence on the arterial pressure. As volume is equal to $\pi r^2 L$, and L is constant for blood vessels, volume depends strongly on vessel radius changes in the venous system.

As we saw that vessel radius changes in the high pressure part of the circulation controls the peripheral resistance, now we see that vessel radius changes in the lower pressure parts, controls the blood volume.

2.3.4 Baroreflex on contractility

Increasing the contractility of the heart will cause an increase in stroke volume, and a decrease in ejection time, thereby facilitating ejection and increasing blood pressure. If we look again at equation 2.1 we see that an increase of the stroke volume will result in an increase of blood flow.

All these mechanisms together make the baroreflex an effective and robust blood pressure control system. On the longer term other control mechanisms will take over to control blood pressure.

Figure 2.6 is a diagram of the baroreflex control system as described.

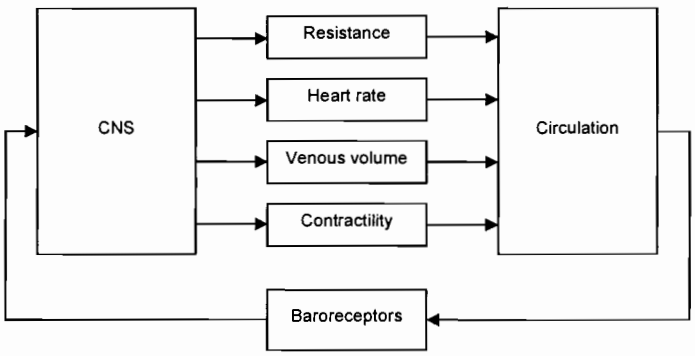

Figure 2.6 *Blood pressure control system structure*

2.4 Blood pressure variability

Looking at the performance of the whole system, we can see that in the normal situation mean blood pressure is quite stable. Blood pressure does not fall measurably when a donor gives 0,5 l blood nor doesn't rise much when 0,5 l blood is rapidly infunded, although cardiac output changes strongly through the reflexes. Also, increasing the cardiac output two fold hardly affects mean arterial pressure. This suggests once more that the baroreflex is a fast, robust, high gain controller.

On the other hand however, the blood pressure level shows a cyclic 24 hour rhythm which can sometimes span as much as two to one pressure range. Systolic blood pressure can increase 50 % to

100 % during painful stimuli in a matter of a minute [20].

This short term blood pressure variability is in contradiction with the presence of an effective stabilizing baroreflex. Assuming that the baroreflex has a very low gain is not a very satisfactory solution. A more acceptable explanation would be that the baroreflex has a high gain in some situations, low gain in others. In the literature [17, 20] baromodulation has been proposed as a solution to the baroreflex paradox. Feedback gain itself is modulated by the CNS.

Blood pressure shows faster oscillations than those daily fluctuations. A much studied one is the so-called 'ten second rhythm'. Some studies suggested that the explanation for this rhythm could to be the presence of a 0.1 Hz resonance in combination with narrow band random noise in the system. It has been speculated that random baromodulation, random heart rate loop gain and random peripheral resistance modulation can explain blood pressure variability.

Another factor that affects blood pressure is respiration. Respiration causes cyclic variations in intra thoracic pressure. This negative pressure strengthens the venous flow toward the heart and thereby modulates the blood pressure.

2.5 Other control mechanisms

We determined the baroreflex as most important in the normal pressure range as it is a fast and powerful reflex. However, at lower pressure ranges and larger time scales, other mechanisms complement control as can be seen in figure 2.4. The mechanisms we will discuss here are the chemoreceptor reflex, the cardiopulmonary reflex and stress relaxation.

Chemoreceptor control mechanism has similarities to the baroreceptor mechanism. However, the chemoreceptors are excited by a decreased blood flow. This excitation is not significant until arterial pressure falls below approximately 60 mmHg [4]. The receptor mechanism relies on measurement of CO_2 concentration. The reflex causes similar sympathetic excitation as the baroreceptors, and prevent a further fall in pressure. The chemoreceptor mechanism is of almost no value as a pressure control mechanism in the normal pressure range. However, when the arterial pressure falls below 60 mmHg, this mechanism can become significant in controlling pressure.

The cardiopulmonary reflex is initiated by receptors in the low pressure areas of the heart, central veins and the pulmonary vessels. Stretch of these receptors is caused by blood volume changes in these low pressure areas. The effectors modulate peripheral resistance and heart rate, and thus influence arterial pressure. The reflex can be seen as a feed-forward pressure controller because signals from low-pressure areas are fed forward to control pressures in the high pressure area. In the normal pressure range it may play a significant role.

Stress relaxation is the phenomenon that occurs at normal pressure ranges but is a relatively slow

mechanism. This mechanism is no control system like the others but is a vessel property (visco-elasticity). When the blood volume in a vessel is increased step-wise the pressure will first rise step-wise, but the stress relaxation will make the pressure gradually drop towards the value before the volume step. All vessels in the human body show stress relaxation, though the effect is mainly observed in the systemic veins [5].

2.6 Model considerations and constraints

In all modeling efforts considerations with respect to the described aspects and choices with respect to the constraints have to be made. Below our main considerations are summarized.

Beat-to-beat or continuous
For some studies beat-to-beat models with a corresponding elementary model description satisfy. In this study we want to look at pulsatile effects in the circulation and compare them with pulsatile measurements in humans, so it is necessary to develop continuous model.

Closed circulation or open circulation
We are mainly interested in pressures and flows in the aorta. But we also want to study the volume shift effects in the circulation. Thus, we cannot suffice with only a ventricle and aorta model. We will develop a closed transmission line model of the circulation, yet will use simplified models for some of the complex vessel systems like the pulmonary circulation.

Time domain
We are interested in pulsatile waveforms however not with an accuracy in the order of milliseconds. On the other hand we also want to study blood pressure responses during several minutes, but not important are daily rhythms.

Frequency domain
We aim to study blood pressure variability in the frequency band of 1 mHz to 1 Hz. Fluctuations with other frequencies are not investigated.

As a result of these considerations, detailed hemodynamics of the blood vessels are left out. We only implemented baroreflex dynamics and added a simple cardiopulmonary reflex. The structure of our model is given in figure 2.7.

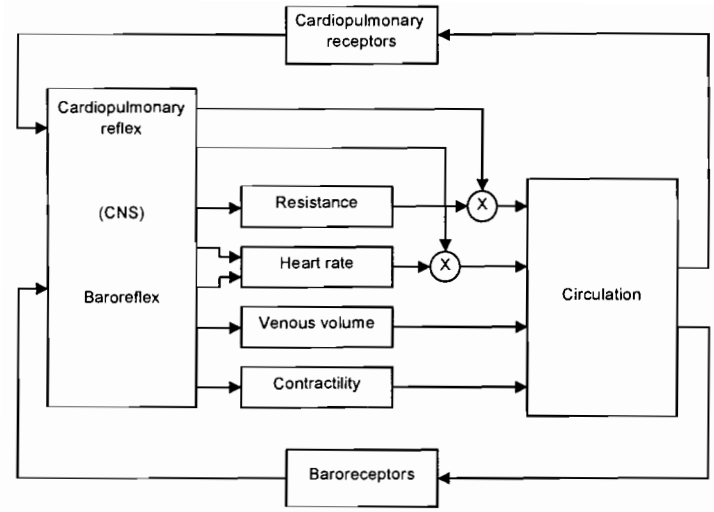

Figure 2.7 *Detailed structure of the control system*

Chapter 3 Circulation model

3.1 model structure

In chapter 2 we described the different parts of the blood circulation and pressure regulation system and showed a diagram of the structure (fig 2.7). The model we use for simulation has a similar structure. In the following chapters, we will describe how we implemented the different parts in our model. This chapter describes the mathematics of our circulation model.

3.2 General approach

The model we used for the circulation is a so-called transmission line model. In a transmission line model, a finite number of segments are lumped into a cascade, with each segment describing a specific part of the circulation. Increasing the number of segments improves the behavior of the model, because the parameters of each segment can be fine-tuned to meet the local vessel and wall characteristics. However, this also increases model complexity and the computation time so there is a trade off between model performance and computation time.

3.2.1 Windkessel element

The basic element we used for lumping is based on the windkessel theory. This windkessel theory conceives the blood vessels as a system of interconnected elastic tubes with fluid storage capacity. The electrical equivalent of such a windkessel segment is shown in figure 3.1.

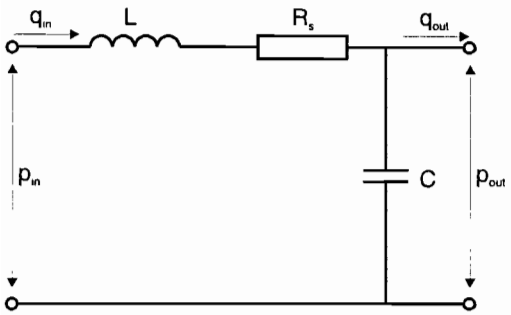

Figure 3.1 *Electric equivalent of the Windkessel model of a blood vessel*

The meaning of the electric elements in this model can be seen for a blood vessel model as follows. L is the fluid inertance, R_S is the viscous drag resistance and C the vessel wall compliance. Current and voltage are the equivalents of flow and pressure.

As the pressure in the vessel rises, the diameter of the vessel will increase. The mathematical relations describing the windkessel model are shown in equation 3.1, 3.2 and 3.3.

$$p_{out} = \frac{V - V_{dead}}{C} \tag{3.1}$$

$$V = \int q_{in} \; q_{out} \; dt \tag{3.2}$$

$$q_{in} = \frac{1}{L} \int p_{in} - p_{out} - q_{in} \; R_S \; dt \tag{3.3}$$

With p_{in} and p_{out} the pressure at the beginning and the end of the vessel segment, and q_{in} and q_{out} the flow at the beginning and the end of the vessel segment. V is the volume of the vessel and V_{dead} is the unstretched volume. With this we mean the volume of the vessel when no pressure is present.

The segment is modeled in such a way that its inputs are input pressure and outflow and its outputs are output pressure and inflow. Additionally the volume of the segment can be regarded as a third output. The black box of a segment is shown in figure 3.2.

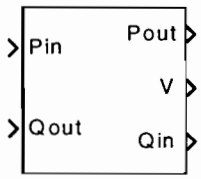

Figure 3.2 *Black-box scheme of a circulation segment*

Now that we have described the general segment, we have a block with which we can build a model of the circulation. Firstly, lumping should be done in such a way that the beginning and the end-point correspond with clearly identifiable anatomical locations. Another guide rule when lumping is the equal cutoff frequency principle. The L shaped segmental model of figure 3.1 is in fact a lowpass filter. Frequencies beyond the lowpass cutoff frequency become attenuated. The segments must be modeled in such a way that these cutoff frequency are all in the same order.

3.2.2 The windkessel characteristics

To derive the transfer function of the model we can rewrite equation 3.1, 3.2 and 3.3 with the Laplace transform as follows:

$$\begin{cases} p_o = \dfrac{1}{sC}\left[q_i - q_o\right] \\ q_i = \dfrac{1}{sL}\left[p_i - p_o - q_i R_S\right] \end{cases} \tag{3.4}$$

$$\begin{cases} p_o = \dfrac{1}{1 + s^2LC + sR_SC}\, p_i - \dfrac{R_S + s[L + R_SC]}{1 + s^2LC + sR_SC}\, q_o \\ q_i = \dfrac{sC}{1 + s^2LC + sR_SC}\, p_i + \dfrac{1}{1 + s^2LC + sR_SC}\, q_o \end{cases} \tag{3.5}$$

Looking at the denominators of equation 3.5 we find the corresponding parameters for the system:

$$\begin{aligned} \omega_n &= \frac{1}{\sqrt{LC}} \\ \zeta &= \frac{R_S}{2}\sqrt{\frac{C}{L}} = \frac{1}{2Q} \end{aligned} \tag{3.6}$$

With ω_n the undamped natural frequency and ζ the damping ratio. The input impedance of the system at closed output ($q_0 = 0$) is defined as input pressure over input flow. From equation 3.5 the Laplace representation of the input impedance can be derived as:

$$Z(j\omega) = \frac{(j\omega)^2LC + j\omega RC + 1}{j\omega C} \tag{3.7}$$

A Bode plot of this input impedance is shown in figure 3.3.

From the amplitude spectra the low pass behavior becomes clear. We can see that all frequencies above 2 Hz are heavily attenuated

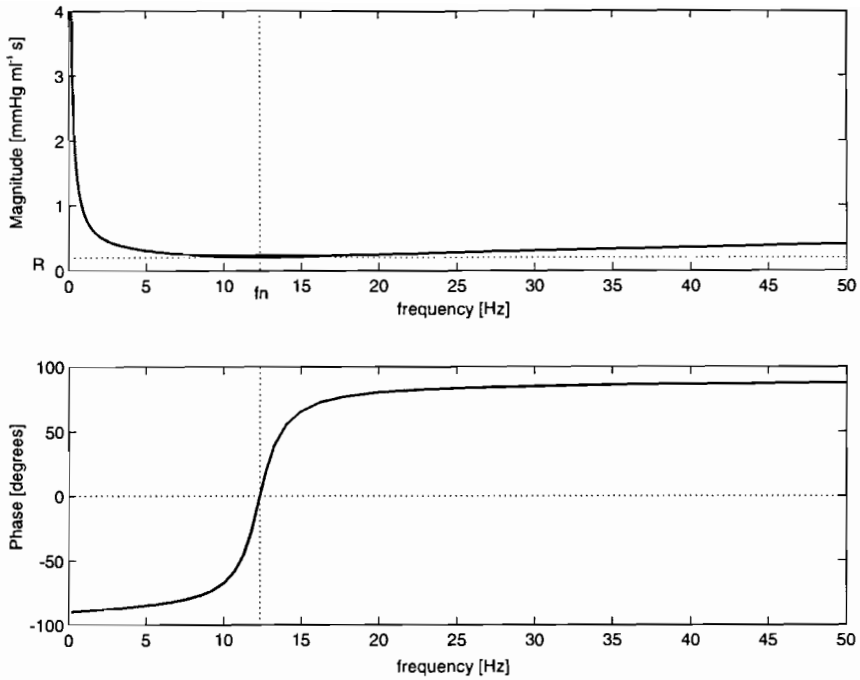

Figure 3.3 *Bode plot of the input impedance of a Windkessel element*

3.3 Modeling blood vessels

The model described until now is a general segment that can be used to simulate a certain blood vessel. To make a model of the circulation we are going to put these segments in a cascade of segments and connect the last segment to the first segment. All segments represent a specific part of the circulation. We divided the circulation into the following parts: systemic arteries, systemic veins, right atrium, tricuspid valve, right ventricle, pulmonary valve, pulmonary arteries, pulmonary veins, left atrium, mitral valve, left ventricle and aortic valve. For all segments, we will use a windkessel-based model.

This approach however implicates several simplifications of the real behavior. Compared to a blood vessel the model is simplified as follows. The model compliance that simulates the blood vessel compliance is simulated as a pressure independent compliance. Yet blood vessel compliance is a function of both pressure and time. These two properties are described in the following two sections. The heart model segments differ even more from the standard windkessel model. The adjustments we made to the heart segments are described in the third section.

3.3.1 Non-linearity in the aorta

The general model of figure 3.1 uses all linear elements independent of pressure and volume in the vessel. In practice, the vessel wall will become stiffer with increasing volume and the resistance will become smaller with increasing volume. This occurs in all blood vessels to some degree. We implemented this only for the aorta model. Two of the model parameters, characteristic impedance (R_S or Z_0) and arterial compliance (C), can be derived from an aortic pressure-area relationship. The characteristic impedance Z_0 can be expressed as:

$$Z_0 = \sqrt{\frac{\eta}{A\ C'}} \qquad (3.8)$$

Here η is the density of blood, A is the cross-sectional area of the aorta, and C' is the aortic compliance per unit length. C' is the derivative of the pressure-area relation ship with respect to pressure (p)

$$C' = \frac{dA}{dp} \qquad (3.9)$$

$$C = l\ C' \qquad (3.10)$$

Compliance C represents the lumped compliance of the entire arterial system. We assume its value to be equal to the compliance of one unit length of thoracic aorta times an effective aortic length, l. As we can see, Z_0 and C are represented in terms of the aortic pressure-area relationship and its derivative. We used the arctangent model of aortic mechanics of Langewouters [5]. According to Langewouters et al, the cross-sectional area can be described as a function of pressure by an arctangent with three parameters

$$A(p) = A_m \left\{ \frac{1}{2} + \frac{1}{\pi} \arctan\left(\frac{p - p_0}{p_1} \right) \right\} \qquad (3.11)$$

A_m is the maximal cross-sectional area at very high pressure. Parameter p_0 defines the position of the inflection point on the pressure axis (fig. 3.4). p_1 defines the width between the points at one-half and three-quarter amplitude (fig. 3.4). Parameters p_0 and p_1 compare with the mean and the SD of a probability function.

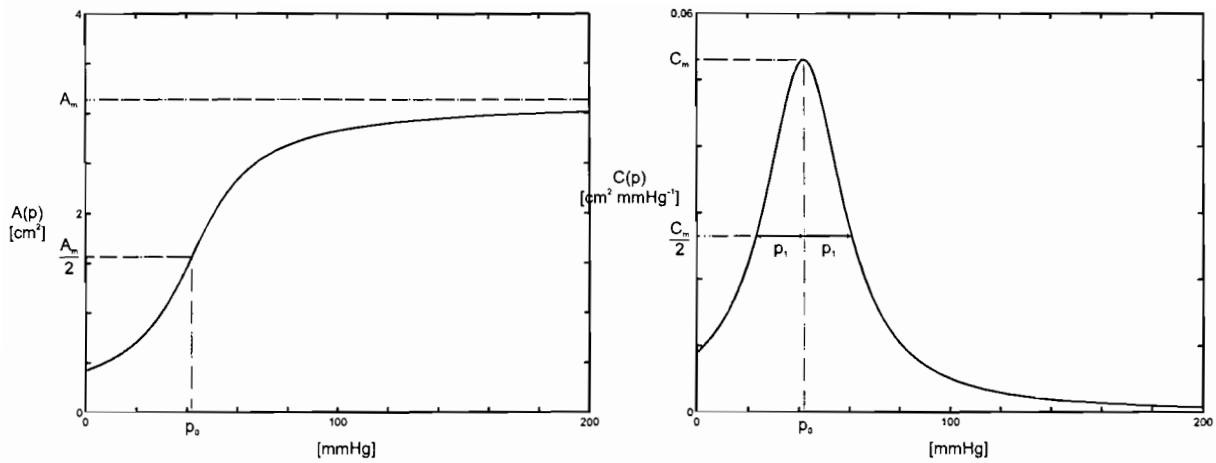

Figure 3.4 *Plots of the cross sectional area of a human aorta (left) and the compliance per unit length of a human aorta (right) both as a function of pressure.*

The compliance per unit length is the derivative of $A(p)$ with respect to p (eq. 3.12) and depends on p

$$C'(p) = \frac{dA}{dp} = \frac{C_m}{1 + \left(\frac{p - p_0}{p_1} \right)^2} \quad , \quad C_m = \frac{A_m}{\pi \, p_1} \tag{3.12}$$

Langewouters [5] investigated the age dependency of the parameters and found the following equations for the parameters.

Table 3.1 *equations for arctangent aortic model parameters vs. Patient age, weight , height and gender.*

Parameter	Male ♂	Female ♀
A_m [cm²]	562	412
p_0 [mmHg]	71.7 - 0.892A	75.8 - 0.892A
p_1 [mmHg]	57.2 - 0.452A	55.6 - 0.413A

Here is A_m, maximal area; p_0, inflection pressure; p_1, width parameter; A, patient age.

Given correct values for the arctangent parameters l, A_m, p_0 and p_1, the model parameters Z_0 and C can be computed for any pressure p.

3.3.2 Visco-elasticity in the blood vessel model

The three-element model used until now describes the static mechanical properties of a blood vessel. The vessel was seen as a fully elastic tube according to the windkessel approach. If we want to model the dynamic properties of human blood vessels, we have to extend the model with visco-elasticity. This means that besides the elasticity of the vessel also a damping must be included. Langewouters [5] has studied this dynamic behavior of the aorta. As a result, he extends the static compliance to a dynamic compliance. The second order equation for this compliance is defined as follows:

$$C(t) = C\left(1 - \alpha_1 e^{-t/\tau_1} - \alpha_2 e^{-t/\tau_2}\right) \qquad (3.13)$$

In other words, the compliance of a vessel is a time-dependent quantity which approaches its static value C, only for large t. The time constants Langewouters finds for the aorta, range from about 1 s for the first to 15 s for the second. As we are only interested in the pulsatile behavior we leave the 15 s time constant out. The electric equivalent for the dynamic compliance is shown in figure 3.5.

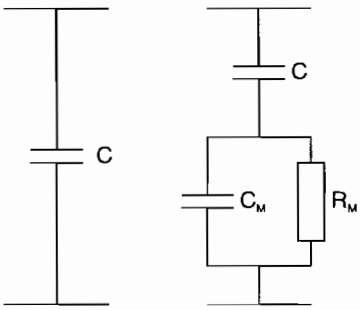

Figure 3.5 *Electrical equivalent of a pure elastic tube (left) and a visco-elastic tube (right)*

With equation 3.13, we find for the visco-elasticity elements that:

$$C_M = \frac{1 - \alpha}{\alpha} C$$
$$R_M = \frac{\alpha\tau}{C} \qquad (3.14)$$

Langewouters found the following parameters values:

Table 3.2 Parameter values for the visco-elastic model

Parameter	value
α	0.08 ± 0.02
τ [s]	0.7 ± 0.2

3.4 Modeling the heart

The dynamics of a heart chamber are quite different from other vessels, since they are contracting actively.

3.4.1 Ventricles

During diastole, the cardiac muscle relaxes and the heart fills with blood. During systole the cardiac muscle contracts and the heart empties, the cardiac walls become stiffer and the volume of the ventricles changes. During this phase the pressure rises quickly and blood flows out. These different states can also be illustrated looking at the pressure volume loop of the ventricles, shown for the left ventricle in figure 3.6

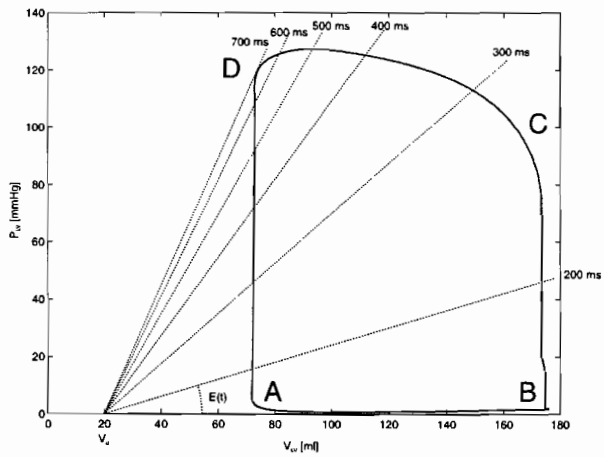

Figure 3.6 *Pressure volume curve of the left ventricle. The slope of the dashed lines denotes the elastance at the different times.*

When we start at point *A* of the curve the heart is filled with 70 ml of blood at low pressure. During the filling phase, volume increases to 170 ml at almost constant pressure. At point *B*, the heart is completely filled. At this point, the ventricle starts to contract. At first, this results in a pressure rise without a volume change and at point *C* the ventricle starts to empty. At point *D*, 100 ml of blood has flowed out. The muscle relaxes and pressure drops almost zero at point A at the end of the relaxation

phase. This cycle is repeated every heart beat.

Modeling this behavior we used the time-varying elastance concept, developed by Suga and Sagawa [13]. A time-varying elastance $E(t)$ is defined as:

$$E(t) = \frac{p_v(t)}{V(t) - V_{dead}}$$

Where $p_v(t)$ denotes ventricular pressure, $V(t)$ ventricular volume and V_{dead} a dead volume equivalent to ventricular volume at zero transmural pressure. The slopes of the dashed lines in figure 3.6 denote the elastance at the different points in the cycle.

Kass et al [9] have measured the pressure volume curves in many different patients and concluded that the time-varying elastance can be characterized with a normalized curve that fits all patients. This elastance curve is approximated by Westerhof et al. [11] with the following periodic double Hill function.

$$E(t) = E_{\max}\left\{ a \left[\frac{\left(\frac{t}{\alpha_1 T} \right)^{n_1}}{1 + \left(\frac{t}{\alpha_1 T} \right)^{n_1}} \right] \cdot \left[\frac{1}{1 + \left(\frac{t}{\alpha_2 T} \right)^{n_2}} \right] \right\} + E_{\min} \qquad (3.16)$$

This curve is shown for a single heart beat in figure 3.7

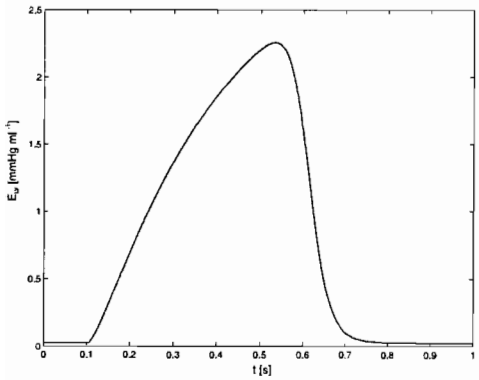

Figure 3.7 *Modeled left ventricle elastance as function of time.*

Dimensionless shape parameters α_1 and α_2 define the relative appearance time of each curve within the heart period, T, and exponents n_1 and n_2 determine the steepness of the ascending and descending parts respectively. The parameter values for the human model are shown in table 3.3

Table 3.3 Parameter values of the varying elastance model

Parameter	Human
Maximum elastance (E_{max}) [mmHg/ml]	2.31 † / 0.37 ‡
Minimum elastance (E_{min}) [mmHg/ml]	0.06 † / 0.01 ‡
Unstretched volume (V_{dead}) [ml]	20
shape factor α_1	0.303
shape factor α_2	0.508
exponent n_1	1.32
exponent n_2	21.9

† value for left ventricle

‡ value for right ventricle

3.4.2 Atria

The role of the atria is less important than that of the ventricles. With their volume five times smaller then the ventricles and their small contribution to the heart cycle they can be seen as an extension of the veins. We have not separately modeled the atria but included their compliance into the compliance of the veins.

3.4.3 Valves

Four valves are present in the heart: the tricuspid valve (between right atrium and right ventricle), the pulmonary valve (between right ventricle and pulmonary artery), the mitral valve (between left atrium and left ventricle), and the aortic valve (between left ventricle and aorta). The mitral and the tricuspid valve prevent back-flow of blood into the atria during ventricular systole. The aortic valve and pulmonary valve prevent back-flow of blood from the circulation into the ventricles during diastole.

The model we use for the valves is a pressure and flow-controlled switch. When the pressure difference over the valve is above a specified value the valve is open and connects the ejecting heart chamber with the output compartment. When the flow reaches a specified negative value the valve closes. This is shown in the state diagram of figure 3.8.

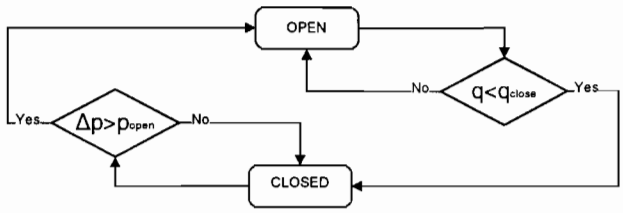

Figure 3.8 *State diagram of the heart valve model*

The parameters q_{close}, which is the flow value at which the valve closes, and p_{open}, which is the value of the pressure difference at which the valve opens, are different for all four valves. The electrical equivalent is a simple rule-controlled switch.

The model of the aortic valve differs from the above described model as follows. When the flow through the open valve becomes negative the back-flow through the valve is integrated. When the integrated back-flow has reached the volume necessary to close the valve the switch is opened and the ejecting chamber is separated from the left ventricle. The corresponding state diagram is shown in figure 3.9.

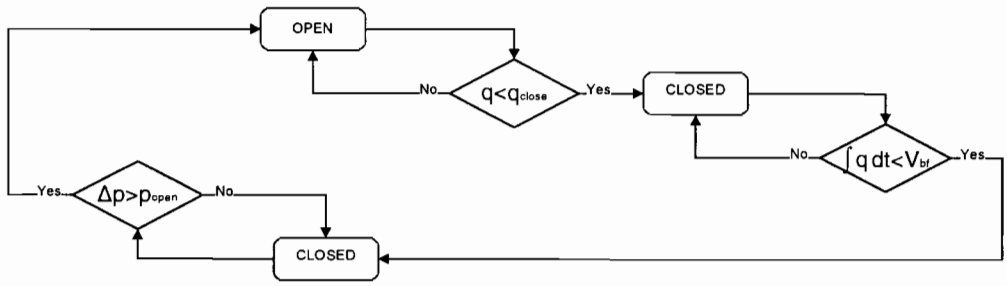

Figure 3.9 *State diagram of the aorta valve model*

Besides this, we also added a valve compliance. The valve compliance mimics the bending valve area when it is closed. From experiments, we found that a C_{vlv} of 0.1 ml · $mmHg^{-1}$ leads to satisfactory simulation results. The electrical equivalent is shown in figure 3.10.

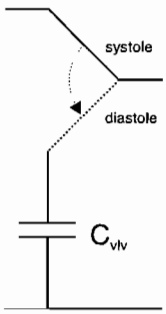

Figure 3.10 *Electric equivalent of the aortic valve*

***Table 3.4** Values of the heart valve models*

Valve	q_{close} [ml/s]	p_{open} [mmHg]	$V_{backflow}$ [ml]
Mitral valve	-150	4	-
Aorta valve	0	0	0.05
Tricuspidal valve	-37.5	0	-
Pulmonary valve	-37.5	0	-

3.5 Complete model

In the preceding sections we first described the general segment model and then the adjustments for certain circulation segments. The complete circulation model we obtained is shown in figure 3.11. The various parameter values for the different parts are given in table 3.5

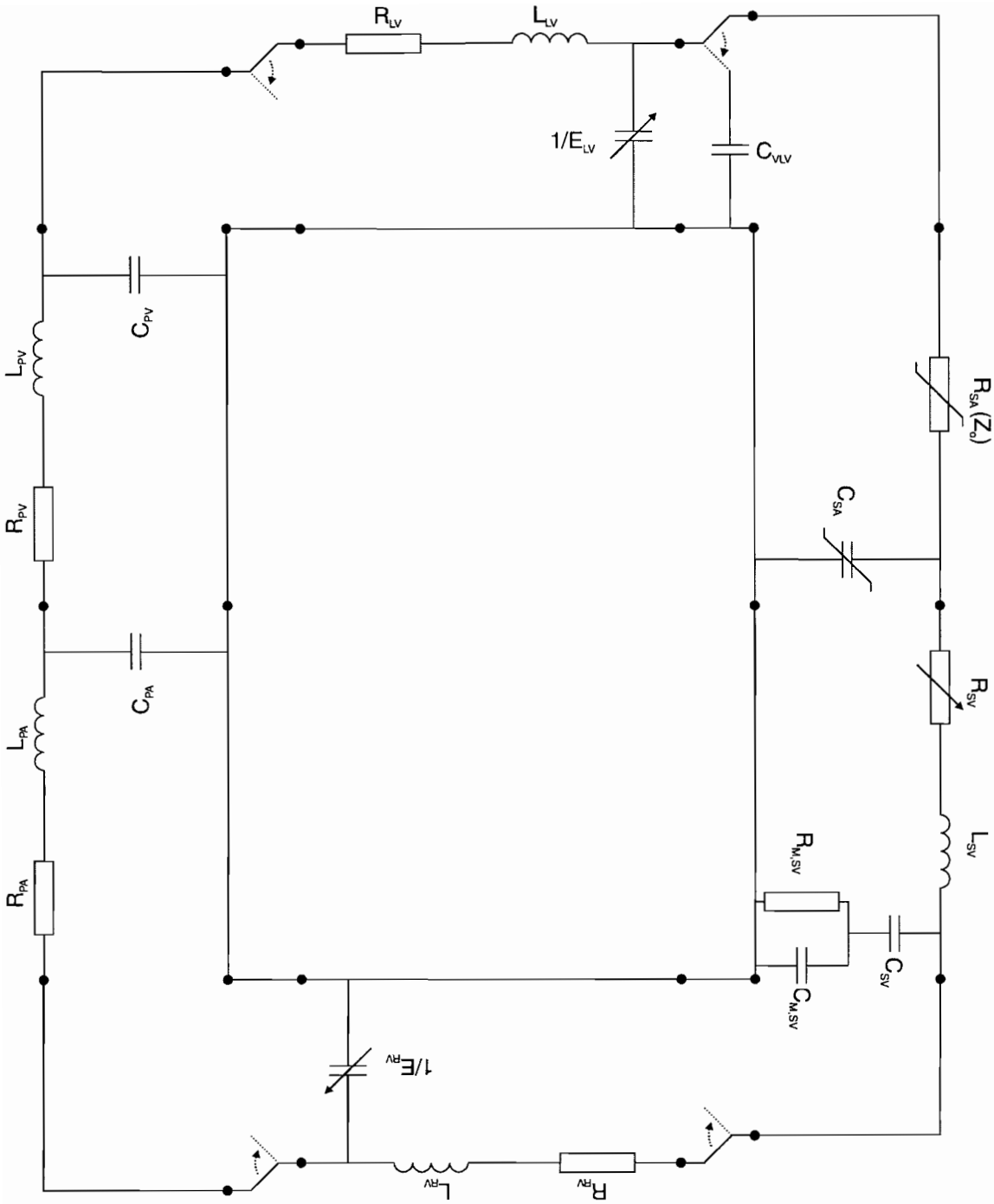

Figure 3.11 *Electric equivalent of the circulation model*

Table 3.5 *Values and parameters of the parts of all segments of the circulation model*

segment	elements	value
systemic arterial segment (aorta)	non-linear resistance (Z_0) non-linear compliance (C)	$\begin{cases} A_m = 5.62\ cm^2 \\ p_0 = 21.8\ mmHg \\ p_1 = 30.1\ mmHg \end{cases}$
systemic venous segment	resistance (R_s) controlled by baroreflex	$R_s = 0.95\ mmHg \cdot s \cdot ml^{-1}$
	visco-elastic compliance (C, C_M, R_M)	$\begin{cases} C = 80\ ml \cdot mmHg^{-1} & V_{dead} = 3000\ ml \\ C_M = 48\ ml \cdot mmHg^{-1} & V_{dead,M} = 100\ ml \\ R_M = 0.625\ mmHg \cdot s \cdot ml^{-1} \end{cases}$
	fluid inertance (L)	$L = 0.005\ mmHg \cdot ml^{-1} \cdot s^2$
right atrium	-	-
right ventricle	resistance (R_s)	$R_s = 0.024\ mmHg \cdot s \cdot ml^{-1}$
	time varying compliance ($C=1/E(t)$)	$\begin{cases} E_{max} = 0.37\ mmHg \cdot ml^{-1} \\ E_{min} = 0.01\ mmHg \cdot ml^{-1} \\ V_{dead} = 20\ ml \\ \alpha_1 = 0.303 \\ \alpha_2 = 0.508 \\ n_1 = 1.32 \\ n_2 = 21.9 \end{cases}$
	fluid inertance (L)	$L = 0.0055\ mmHg \cdot ml^{-1} \cdot s^2$
pulmonary arterial segment	resistance (R_s) compliance (C) fluid inertance (L)	$R_s = 0.015\ mmHg \cdot s \cdot ml^{-1}$ $C = 9\ ml \cdot mmHg^{-1}$ $V_{dead} = 75\ ml$ $L = 0.0005\ mmHg \cdot ml^{-1} \cdot s^2$
pulmonary venous segment	resistance (R_s) compliance (C) fluid inertance (L)	$R_s = 0.1\ mmHg \cdot s \cdot ml^{-1}$ $C = 9\ ml^{-1} \cdot mmHg^{-1}$ $V_{dead} = 150\ ml$ $L = 0.002\ mmHg \cdot ml^{-1} \cdot s^2$
left atrium	-	-
left ventricle	resistance (R_s) time varying compliance ($C=1/E(t)$) fluid inertance (L)	$R_s = 0.02\ mmHg \cdot s \cdot ml^{-1}$ $\begin{cases} E_{max} = 2.31\ mmHg \cdot ml^{-1} \\ E_{min} = 0.025\ mmHg \cdot ml^{-1} \\ V_{dead} = 20\ ml \\ \alpha_1 = 0.303 \\ \alpha_2 = 0.508 \\ n_1 = 1.32 \\ n_2 = 21.9 \end{cases}$ $L = 0.00138\ mmHg \cdot ml^{-1} \cdot s^2$

Chapter 4 Control model

4.1 model structure

In chapter 2 we saw that the control system consists of several different control mechanisms. The baroreflex is the most important control mechanism for short time analysis and in normal pressure range. Therefore, we will focus on the baroreflex.

The baroreflex is initiated by stretch receptors (baroreceptors). As a reaction to increases in arterial pressure the baroreceptors transmit signals into the nervous system. In response, control signals are transmitted through the autonomic nervous system to three areas: heart, systemic veins and arterioles. The model we used is based on the model of Walstra et al. [16] which has been thoroughly verified. In the next sections we will describe how the different parts of the baroreflex are implemented in our simulation model.

4.2 Baroreceptors

As mentioned the baroreceptors are stretch sensors. Increases in arterial pressure raise the stretch in the arterial wall. As a result to this increasing stretch the receptors activate the efferent nerves with impulses. The firing frequency depends on the stretch in the arterial wall. This is also illustrated in figure 4.1.

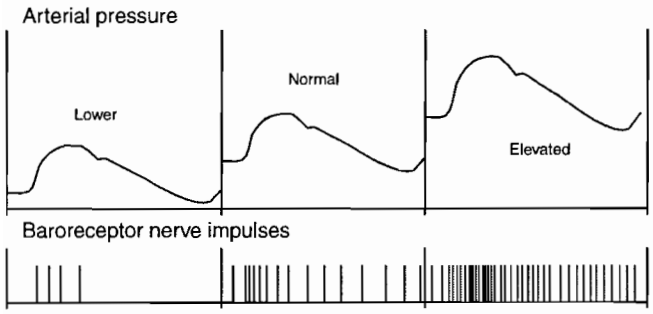

Figure 4.1 *Baroreceptor activity response to arterial pressure*

Besides a static behavior there is also a dynamic behavior. The baroreceptor activity responses are greater for fast fluctuations in arterial pressure. The static and dynamic behavior are separately

described in the following sections.

4.2.1 Static behavior

With static we mean a constant arterial pressure during a few seconds to a few minutes. Walstra [16] finds, according to measurements in dogs, a S-shaped baroreceptor curve for humans. We used a similar curve that is illustrated in figure 4.2.

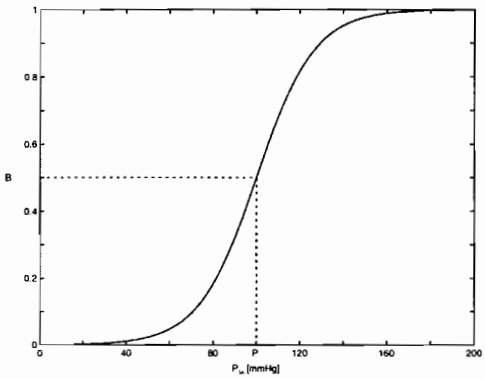

Figure 4.2 Baroreceptor function curve.

Here P_{SA} is the systemic arterial pressure and B is the relative mean baroreceptor activity which is the same as the relative afferent nerve activity. We see that the curve is symmetric around point P=100 mmHg, B=0.5. There is no baroreceptor activity for low pressures, and there is maximum activity (continuos firing) at high pressure. The slope is maximal at the symmetry point. This means that at this point the baroreceptors are most sensitive to pressure changes. The symmetry point can be seen as the target pressure for the control system. It is normally at P_0 = 100 mmHg.

The function curve can be approximated with the following mathematical equation.

$$B = \frac{1}{e^{-0.075\ (P_{SA} - P_0)} + 1} \qquad (4.1)$$

As we see in figure 4.1 the receptor activity is highest at the start of every heart beat. For this reason we decided to take the arterial pressure half way between its systolic and diastolic value, as input pressure for the receptors. The mid-pressure can be calculated when systolic pressure is reached, thus the delay is minimized.

4.2.2 Dynamic behavior

Besides the static behavior there is a time-dependency of the baroreceptor activity. For fast pressure changes (about 0.1 s rise time) the receptors are more sensitive (rate sensitivity) than for slow changes. This can be illustrated by looking at the baroreceptor response to a step-wise pressure increase. The step response is shown n figure 4.3.

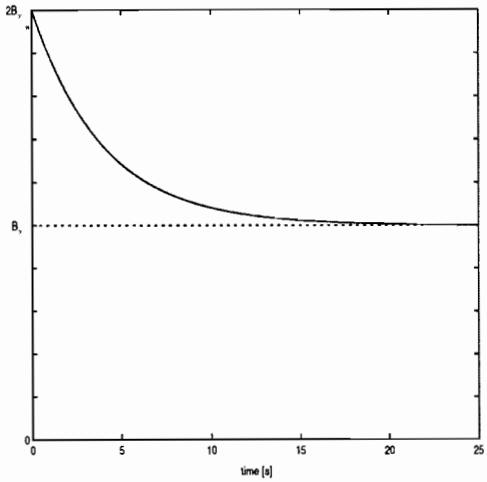

Figure 4.3 *Stepresponse of the baroreceptor activity*

Here B_∞ is the static relative baroreceptor activity for the end pressure. According to measured step response the dynamics can be estimated. Described in the Laplace domain we get the following mathematical equation 4.2

$$B(s) = B_\infty(s)\left(2 - \frac{1}{1+s\,\tau}\right) \qquad (4.2)$$

With $B_\infty(s)$ as defined in equation 4.1. We approximated the step response curve with one time constant. This suits well for our short-term model. The value of τ that is estimated is 4 s.

Beside these fast dynamics, measurements also show that long-term responses to a constant pressure decrease after a few minutes (baroreceptor adaptation or resetting). Because the effect is only present on the very long time-scales of hours and as we are only interested in the short-term behavior, baroreceptor-resetting in not implemented.

4.3 Baroeffectors

The afferent nerve activity from the baroreceptors is conducted to a center in the central nervous system called nuclear tractus solitarii or NTS. These signals are processed to result in efferent nerve activity, which stimulates the quantities (effectors) that are used by the baroreflex to control blood pressure. As described in chapter 1 there are four main baroreflex effectors working at three different

areas. In the next four sections we will describe the model of these effectors.

In all four effector models we used a similar construction. It consists of a time delay that simulates the delay in the CNS and in the afferent and efferent nerves. This is followed by a first order low-pass system that simulates the dynamics of the effector, followed by a gain and an offset. The gain is the open loop gain of the effector branch. The construction is also shown in figure 4.4.

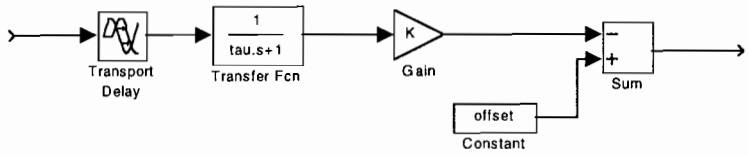

Figure 4.4 *General construction of the baroreflex effector model*

We must bear in mind that modeling the effector this way it is difficult to speak about efferent nerve activity. Taking afferent nerve activity as input and the effected quantity as output does not mean that the nerve activity that is physically between these signals can also be adopted from our block model. The nerve activity is embedded in our system approach.

4.3.1 Baroreflex on heart rate

The heart is innervated both by sympathetic and parasympathetic (vagal) nerves. In the model described by Walstra [16], heart rate was under vagal control only. In healthy awake humans at rest the baroreflex control of the heart is predominantly mediated by enhancement or withdrawal of vagal tone. In normal situations sympathetic control of heart rate plays a minor role. However, in extreme situations it can increase heart rate to as much as 200 beats per minute. Therefore we will take both mechanisms in account. The difference in dynamics of both mechanisms forces us to split these in different models.

Both models consist of a pure time delay and a first order low-pass system. The time delay is mainly the delay between afferent and efferent nerve activity, and the central processing time. The first order system describes the dynamics with dynamic parameters time constant and gain. In order to extend the model of Walstra with a sympathetic branch we used the parameters that were used by Ten Voorden [15] in his hybrid model. He used a sympathetic and vagal time delay of respectively 3 and 0,2 seconds. The time constants Ten Voorden finds are respectively 4 and 1 second. The gain we adopted from Walstra with a 1:2 division between respectively sympathetic and vagal stimulation. We can see that the sympathetic mechanism is slow and less powerful mechanism compared to the vagal mechanism

4.3.2 Baroreflex on systemic resistance

The sympathetic nerves have impact on the arterioles by constriction and dilation of the vessels. This so called vaso-constriction and vaso-dilation will cause changes in peripheral resistance and thereby influence blood pressure. Parasympathetic regulation of the peripheral resistance is absent. We adopted Walstra's nervous control model of the arteriolar tone. He used a delay of 3 seconds and a time constant of 6 seconds.

4.3.3 Baroreflex on blood volume

The venous side of the circulation is also innervated by the sympathetic nervous system. Constriction of the venous blood vessels will decrease the total blood volume. The majority of the blood volume is in the venous part of the circulation under a low pressure. Increasing the blood capacity is a powerful mechanism to decrease the blood pressure. The timing of the response is much slower than the other mechanisms. Walstra used a time delay of 10 seconds and a time constant of 60 seconds. Again no parasympathetic innervation is present.

4.3.4 Baroreflex on contractility of the heart

Besides the nervous control of the heart rate the heart is also innervated with other sympathetic signals. The nervous stimulation of the contractility of the heart is another effector of the blood pressure. At normal pressures Walstra finds from the literature that especially the sympathetic enervation is important in the blood pressure system. The parasympathetic innervation is neglected. Walstra used a time delay of 3 seconds and a time constant of 10 seconds.

4.4 Complete model

An overview of the total model we use for the baroreflex control system is given in figure 4.5. The parameters we used are summarized in table 4.1.

Table 4.1 *Parameters of the control model*

		delay time [s]	time constant [s]	gain
Receptor		0	4 (high emphasis)	nonlinear
Heart rate	sympathetic	3	4 (low pass)	0.3 Hz
	vagal	0.2	1 (low pass)	0.72 Hz
Peripheral resistance		3	6 (low pass)	1.42 mmHg·s·ml^{-1}
Venous volume		10	60 (low pass)	1350 ml
Contractility		3	10 (low pass)	0.48

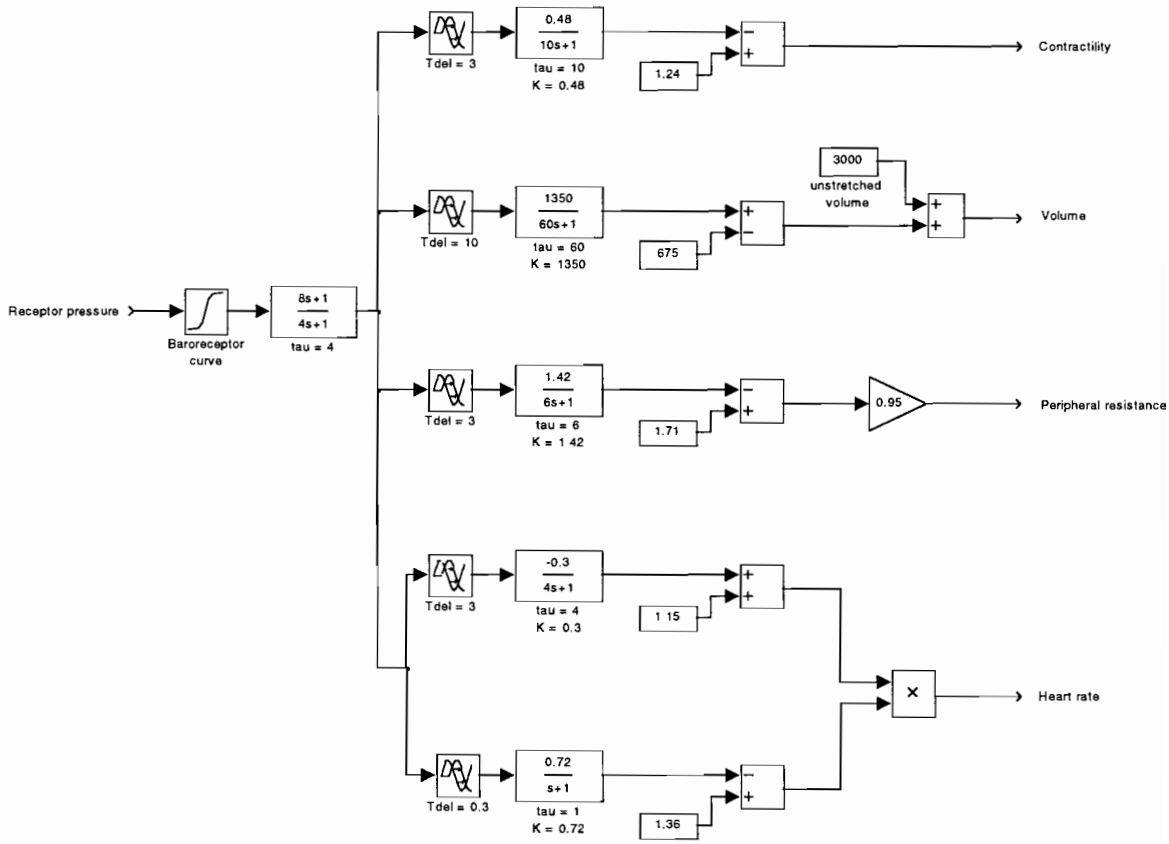

Figure 4.5 *Schematic presentation of the control model*

Chapter 5 Experiments

5.1 Introduction

In the previous chapters we have built our model of the blood-pressure system part by part. In this chapter we will investigate the integration of all parts, and run some simulations to characterize model behavior. When it is possible we compare these experiments with measurements in the human circulation.

First we are going to look at the different signals in the model at rest. We designed our model according to a condition that can be compared with a young healthy man in supine position. The circulation is stable since mean pressures and volumes are constant.

In this situation we first look at pressure and volume levels in the circulation and furthermore we will look at the shape of these curves. When we have assured that these outputs are similar to measurements on the human circulation we test the control system by looking at the open-loop gains.

When we have done this, we will look at the effect of baroreflex gain modulation (baromodulation). We will assign baromodulation as the cause of measured pressure fluctuations. More specific looking at these fluctuations, we will introduce noise sources in the model to explain all frequency components occurring in the blood pressure and heart rate spectra.

5.2 beat-to-beat analysis

With beat-to-beat analysis we mean that we are not looking at signal shapes but only at their mean value during a beat. A start of a beat is defined by the generation of an impulse in the SA-node, the contraction impulse generator, or pace maker, of the heart. Normally this is the moment at which the right atrium starts to contract. In our model, with only ventricles, this means that after every start of the beat there is a period of delay before mechanical activity (contraction) begins.

The beat-to-beat variables are calculated as mean values during a heart beat or maximum and minimum values within a heart beat. The location of the pressures and volumes are chosen in such a way that they agree with anatomic locations. The arteries and veins of both the systemic and the pulmonary circulation as well as both ventricles are chosen. The values are all expressed in medical

units according to table 5.1

Table 5.1 *Used variables with the used medical units and corresponding SI units*

Name	Symbol	Medical unit	SI unit
Pressure	p	mmHg	$1.33 \cdot 10^{2}$ Pa
Volume	V	ml	10^{-6} m^3
Flow	q	ml s^{-1}	10^{-6} m^3 s^{-1}
Time	t	s	s
Resistance	R	mmHg ml^{-1} s	$1.33 \cdot 10^{8}$ kg m^{-4}s^{-1}
Compliance	C	ml mmHg^{-1}	$7.5 \cdot 10^{-9}$ kg^{-1} m^4 s^2
Inertance	L	mmHg ml^{-1} s^2	$1.33 \cdot 10^{8}$ kg m^{-4}
Elastance	E	mmHg ml^{-1}	$1.33 \cdot 10^{8}$ kg m^{-4}s^{-2}
Frequency	f	beat min^{-1} (bpm)	$1.67 \cdot 10^{-2}$ Hz

Measurements in humans arteries yields typical pressure levels of 100 mmHg (systemic circulation) and 15 mmHg (pulmonary circulation) and in the veins 5 mmHg (systemic and pulmonary circulation). In our model we tried to get similar pressure levels as these measured levels. The beat-to-beat values of the different parts of the circulation model are presented in table 5.2.

Table 5.2 *beat-to-beat values of the circulation model at steady state*

		Pressure level [mmHg]		
		min	mean	max
left ventricle				121.2
systemic arteries	begin	77.9	99.1	121.2
	end	77.7	85.4	108.0
systemic veins		4.3	5.2	5.9
right ventricle				22.0
pulmonary arteries		11.3	14.9	17.8
pulmonary veins		2.9	5.7	9.1

Our model contains 4500 ml blood. This total blood volume is held constant during normal simulations (as no blood is infunded or withdrawn). In resting conditions the blood is distributed at the start of every beat (end-diastolic) in the following way:

Table 5.3 *Volumes of the circulation model at steady state*

	End diastolic volumes			
	Unstretched [ml]	stretched [ml]	Total [ml]	[%]
left ventricle	20	117	137	3.0 %
system ic arteries	0	410	410	9.1 %
systemic veins	3000	412	3412	75.8 %
right ventricle	20	102	122	2.7 %
pulmonary arteries	75	142	217	4.8 %
pulmonary veins	150	52	202	4.5 %

Unstretched volume is the volume of a vessel when no pressure is present. As we can see, the veins contain most volume and most of this volume is unstretched volume. This is according to human physiology. In our model the unstretched volume of the arteries are put zero. However, due to the nonlinear relation there is an implicit unstretched volume.

At rest the baroreflex has the following chosen values

Table 5.4 *Values of the control model at rest.*

	value
receptor pressure	100 mmHg
heart rate	60 bpm
peripheral resistance	0.95 mmHg s cm $^{-3}$
maximum contractility	1
unstretched venous volume	3000 ml

Maximum contractility is expressed as a factor upon the normal maximum elastance of both left and right ventricle of respectively 2.31 and 0.37 mmHg ml^{-1}. All other values are in the medical units.

We can also calculate stroke volume and cardiac output according to following definitions.

$$V_S = \int_{t_1}^{t_2} q_{ao}\, dt \qquad (5.1)$$

V_S means stroke volume which is the amount of blood that is pumped out during one heart beat (from t_1 to t_2 in eq 5.1) and Q_H means cardiac output which is the mean outflow of the heart, and f_H is

$$Q_H = V_s \cdot f_H \qquad (5.2)$$

the heart rate and q_{ao} the aorta flow.

We have modeled in such a way that CO and SV agree the normal human values listed in table 5.5

Table 5.5 *Stroke volume and cardiac output in the circulation model at rest*

	value
Stroke volume	100 ml
Cardiac output	100 ml s^{-1} (= 6 l/min.)

5.3 Continuous signals

We will now look at the shape of signals on location where they are well known in real humans. In figure 5.1 the pressures, flows and volumes around the heart are plotted. The left panels for the left side of the heart and the right panel for the right side.

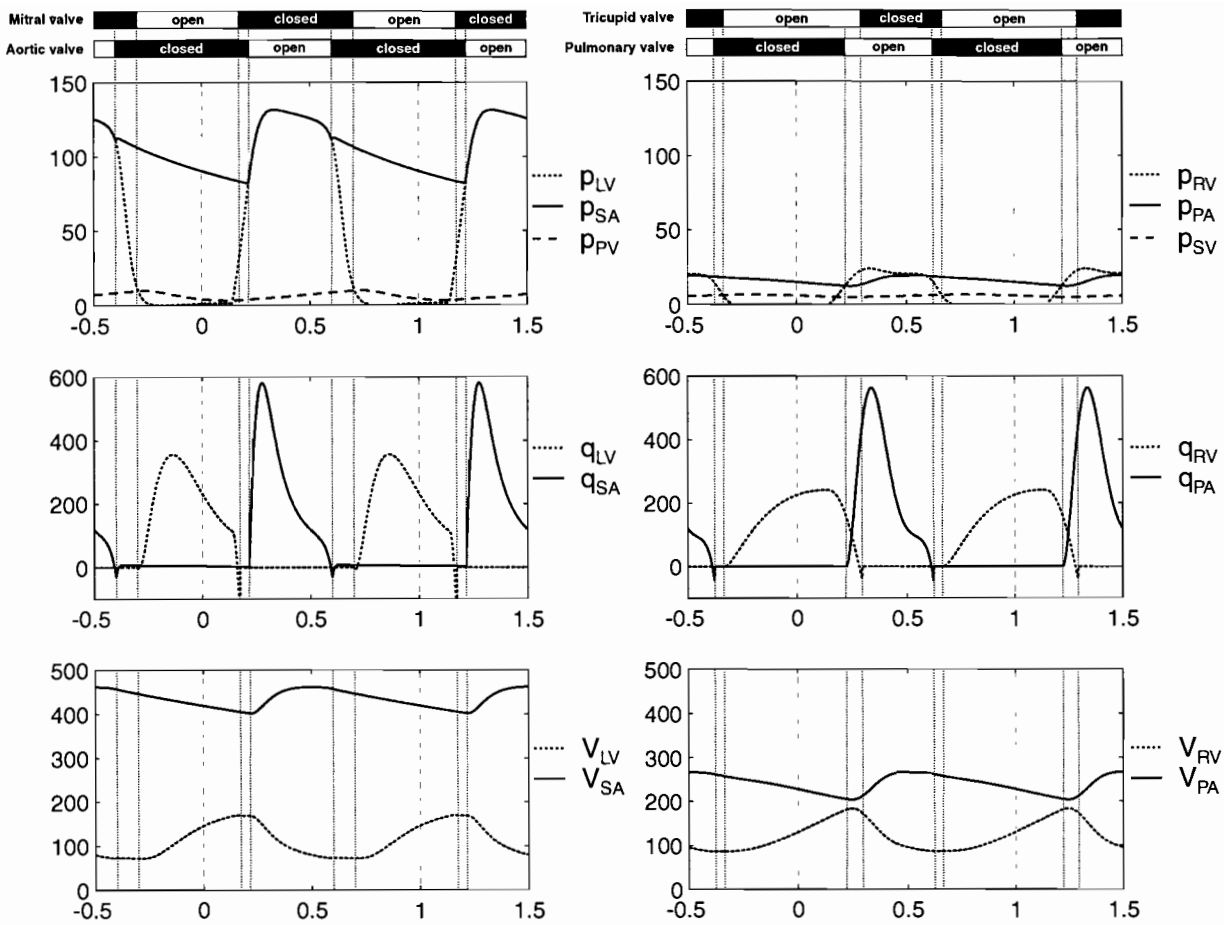

Figure 5.1 *Pressures, flows and volumes in the circulation*

At the start of a heart beat the aortic pressure is slowly descending as the aortic valve is closed and blood flows to the tissues. The ventricle is filled to its end-diastolic volume. When the filled ventricle starts to contract the pressure in the ventricle quickly rises. When ventricular pressure reaches aortic pressure the aortic valve opens and ventricular outflow quickly reaches its peak value from where it similarly descend to zero. Only after some amount blood has back-flowed from the aorta to the ventricle, the aortic valve closes. The ventricle is now emptied approximately to half of its end-diastolic volume. After the ventricle relaxes for some time, the mitral valve opens and the ventricular inflow rises to fill the ventricle. After the ventricle inflow has reached its peak value, the flow is descending again. This ventricle filling is not finished when the next contraction is started. The left ventricle inflow quickly descend and the mitral valve closes quickly after the ventricle contraction. At this time the heart beat cycle starts again.

In the right heart there is a great inertia because of the blood volume of the systemic veins. Consequently the inflow is not stopped when the pulmonary valve is opened. Therefore we get the situation of both ventricle valves being opened at start contraction. The remaining cycle is similar to that of the left part that is described above though pressure levels are much lower than on the left.

5.4 Step responses

Now that we have seen that the circulatory model works properly and that pressure and volume levels reasonably agree to estimates in humans. We will now perform some experiment with circulatory control.

Input of the control system is arterial pressure. In chapter 3 we proposed to use the half up-stroke value of this arterial pressure. In our receptor model we defined a set-point value for the control system. At set point pressure the control system is at rest and no actions are carried out. When input pressure gets above or below the set point value the control system has four effectors that can be used to regulate the pressure toward the set point value. To investigate the response of the controller to pressure variations, we measured the step responses of the control system to a set-point step of 100 to 105 mmHg. The result is given in figure 5.2.

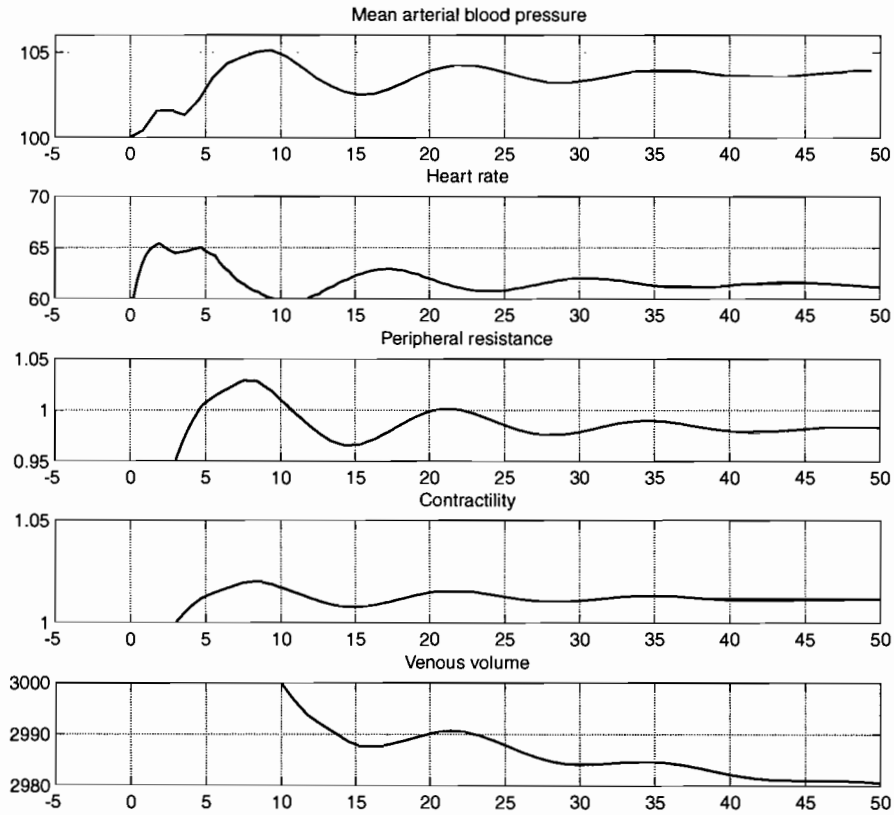

Figure 5.2 *Closed loop step responses of the control system to a receptor pressure step of 100 to 105 mmHg*

We can see that almost immediately after the setpoint step at t=0, the vagal control is activated and heart rate increases causing a moderate pressure rise. After 3 seconds the sympathetic system comes into play which causes a rise in contractility and peripheral resistance. This causes a further rise of arterial pressure.

After some oscillations the arterial pressure reaches its steady state value. The frequency of this oscillation can be estimated as 1/12.5=0.8 Hz. We can see that the slowest effector, venous volume decreases only after 10 seconds. The steady state value of arterial pressure is approximately 104 mmHg at a setpoint value of 105 mmHg. This gives a closed loop DC gain of 4/5=0.8 and an open loop gain of 4. The steady state error is 20 %.

We will now open the loop of the model and determine the response of arterial pressure to variations of receptor pressure. Because of the nonlinear behavior of the model we must operate near the normal work point of the system. Then we will assume that for small variations around this work point we can linearize the behavior. To test this we measured the steady state output of the system at different input values. The result is shown in figure 5.3.

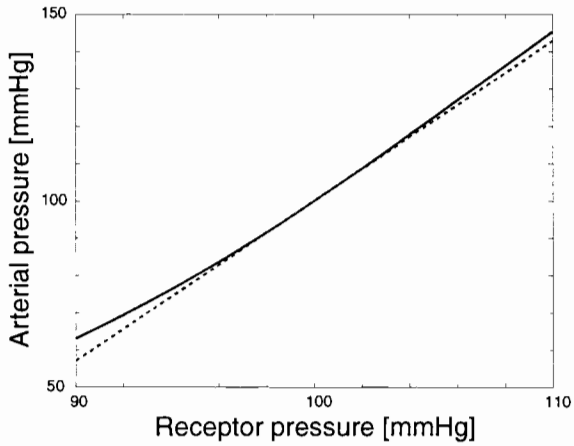

Figure 5.3 *Arterial pressure as function of receptor pressure*

The dashed line denotes the linearization we assume. We see that if we range input pressure with ± 5 mmHg around set point pressure (100 mmHg), the deviation from the linearization is only a few percent.

To calculate DC gain we measure at steady state the mean arterial pressure at 95 and 105 mmHg receptor pressure. To measure the gain of an effector loop every effector is separately made active while the others are fixed to their resting values. Finally all effectors are made active to measure the overall gain. The results are given in table 5.6.

Table 5.6 DC-gains of the effector loop in the control model

Effector loop	DC-gain
Venous volume	2.1
Peripheral resistance	1.9
Contractility	0.13
Heart rate	0.10
All	4.2

We can see that most effective, in terms of loop gain, to regulate blood pressure are changes of volume and resistance. Both effectors have an open-loop DC gain of approximate 2. We can verify this with the following rough estimates.

$$\left.\begin{aligned} B &\approx \alpha_{rec} \cdot p_{rec} \approx 0.019 \cdot p_{rec} \\ R_{per} &= K_R \cdot B = 1.42 \cdot B \\ p_{sa} &\approx Q_H \cdot R_{per} = 100 \cdot R_{per} \end{aligned}\right\} p_{sa} \approx 2.70 \cdot p_{rec} \qquad (5.3)$$

$$\left.\begin{aligned} B &\approx \alpha_{rec} \cdot p_{rec} \approx 0.019 \cdot p_{rec} \\ V_{vol} &= K_V \cdot B = 1350 \cdot B \\ p_{sv} &= \frac{V_{vol}}{C_{sv}} = \frac{V_{vol}}{9} \end{aligned}\right\} p_{sv} = 2.85 \cdot p_{rec} \qquad (5.4)$$

With the following used variables: B Baroreceptor activity, α_{rec} slope of the receptor curve (at 100mmHg), p_{rec} receptor pressure, p_{sa} system arterial pressure, p_{sv} system venous pressure, R_{per} peripheral resistance, K_B baroreflex gain on resistance, K_V baroreflex gain on volume, V_{vol} venous volume, C_{sv} systemic veins compliance.

These calculations are only rough estimates of the gain. We see that the measured gains are of the same order as these estimates. The two other effectors have smaller gains and therefore are less effective, though not less important as we will see later, because they operate in a higher frequency range.

The total DC gain is 4.2. In closed loop the transfer function G(s) can be expressed as the open-loop transfer function H(s) as follows:

$$Y = G(s) \cdot X = \frac{H(s)}{1 + H(s)} X \qquad (5.5)$$

This means that DC gain in closed loop will be 4.2/5.2=0.81. The corresponding steady state error can be estimated as 19.2 %. This agrees with what we estimated from the step responses.

5.5 Loop gains

Besides the static gains we are also interested in dynamic behavior of the system. To this purpose we measure the open-loop gain over a frequency range from 1 mHz to 1 Hz. The amplitude spectra are obtained using a white noise source as an input signal to the baroreceptors. The spectral computations are performed according to appendix A. The result is given in figure 5.4.

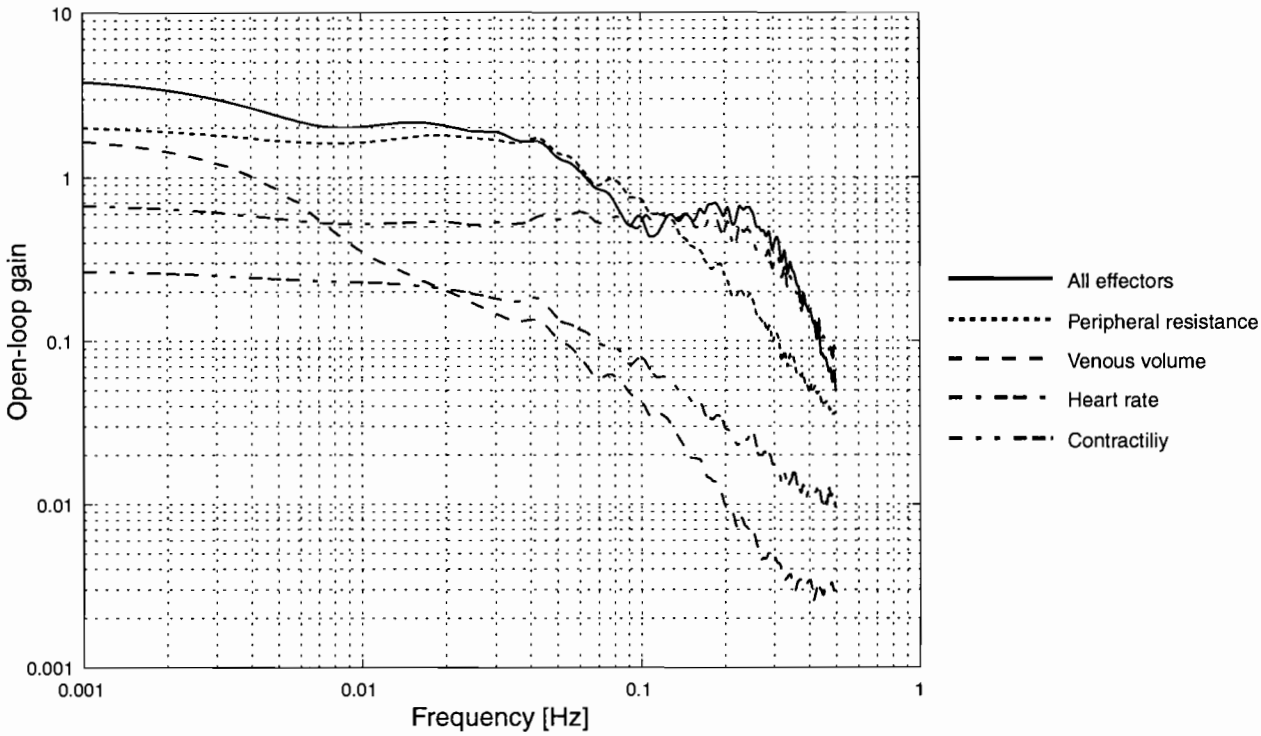

Figure 5.4 *Open loop gain of all effector loops in the model*

We can see that the high gain effector loops have a small bandwidth while the low gain effectors have a higher bandwidth. The gain of the system at each frequency with all effectors active is not equal to the algebraic sum of all effector gains separately. This is due to phase shifts caused mainly by the time delays in the model. From these spectra and the DC gains we can estimate the -3 dB bandwidth for each effector. The results are given in table 5.7

Table 5.7 *Bandwidth of the open loop effector gain in the control model*

Effector loop	Bandwidth (Hz)
Venous volume	0.0025
Peripheral resistance	0.045
Contractility	0.035
Heart rate	0.15
All	0.035

If we close the control loop we measure the closed loop gain of the system. The result is shown in figure 5.5.

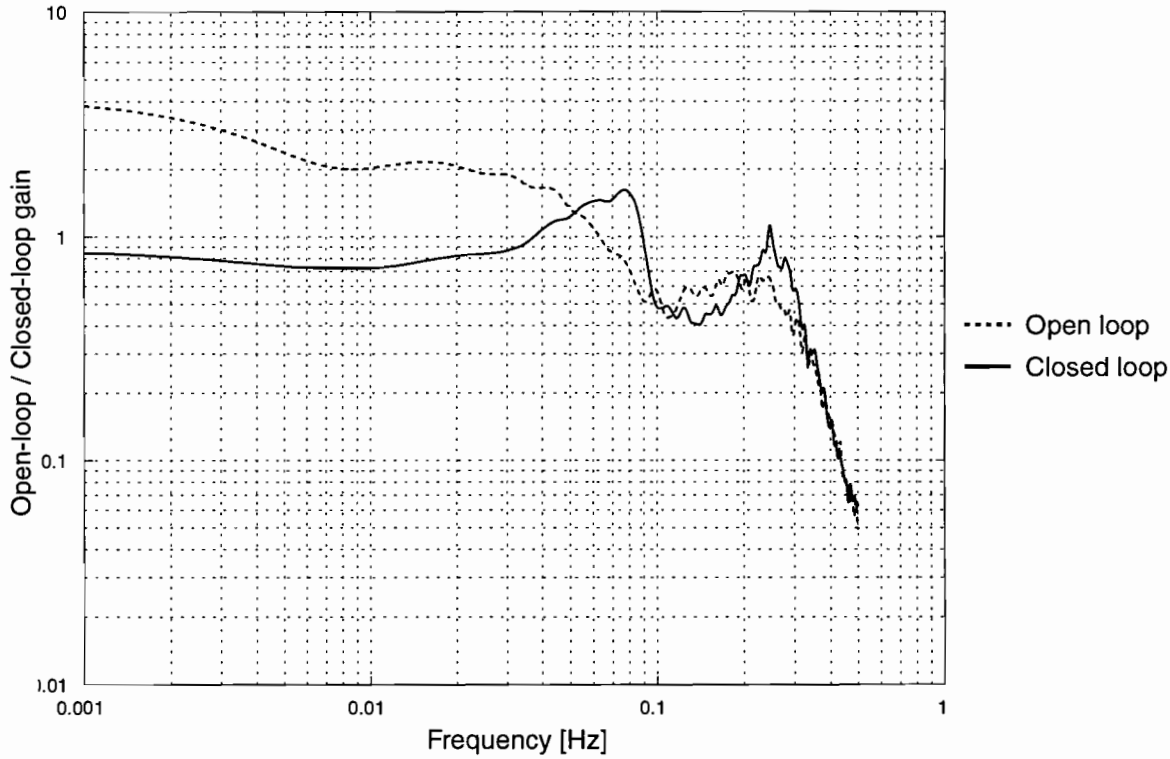

Figure 5.5 *Open and Closed loop gain of the system*

The DC gain that follows from the closed loop simulation agrees with the earlier found value of 0.8. Furthermore a clear resonance peak becomes apparent at approximate 0.08 Hz. The oscillation caused by this resonance occur at approximately 12.5 s periodicity as we also saw in figure 2.5. The second peak in the closed loop gain cannot be explained from physiologic point of view. The resonance phenomenon is discussed in more detailed in the following sections.

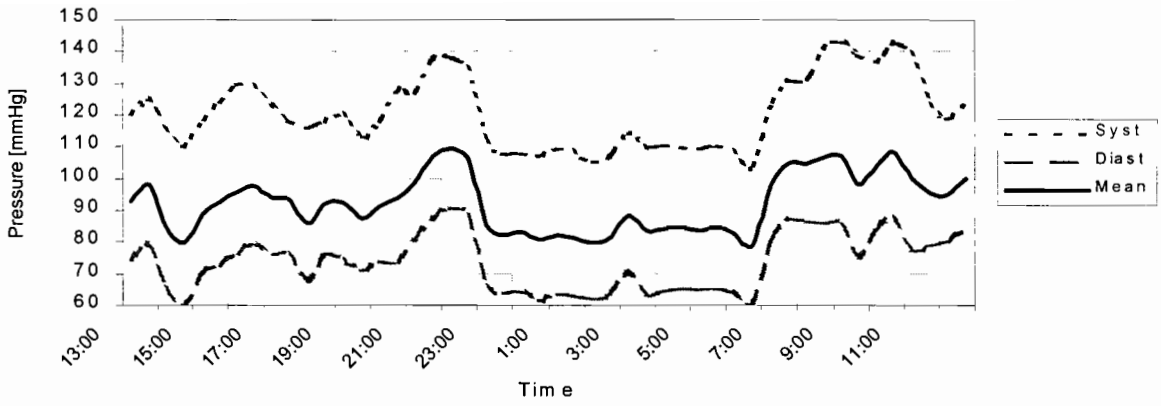

Figure 5.6 *A 24 hour registration of blood pressure*

5.6 Baromodulation

The model behavior shows an effectively stable average blood pressure, due to the relative high gain, plus damped oscillations due to a resonance near 0.08 Hz. Yet continuous registrations over 24 hours show pressure variation that cannot be explained by the model. For example during the 24 hour pressure can respectively fall and rise 20 mmHg in a short time. An example is shown in figure 5.6. Around 0:00 we can see a substantial pressure drop when the patient falls asleep.

Similar pressure changes may occur when patients are subjected to mental stress or pain stimuli. From control theory the obvious way to produce these pressure changes is to change the setpoint of the baroreflex. This process occur in physiology and is called baroreceptor adaptation. It is, however, a passive process with a time constant in the order of 10 hours and thus cannot explain the fast changes observed.

Another parameter in the model that can be modulated easily is gain. Several studies prove the existence of gain modulations in the baroreflex control system. Simulation of this phenomenon yields that increasing the baroreflex gain (baro-facilitation) cause the pressure to fall but not below safe levels, and decreasing baroreflex gain (baro-inhibition) cause a pressure rise to potentially high levels. In figure 5.7 the effect is shown for gain modulation factors of 10 in either direction from normal.

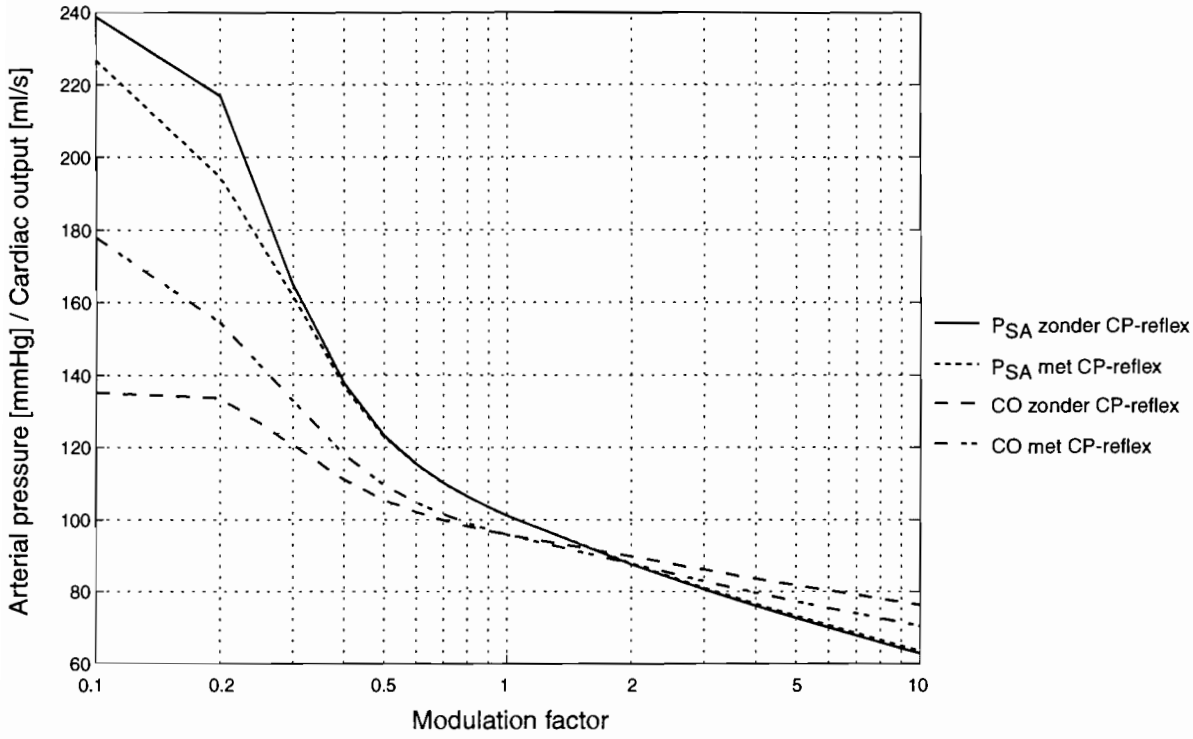

***Figure 5.7** Arterial pressure and cardiac output as function of baromodulation*

Baro-inhibition, causes pressure and cardiac output to rise though at first the rise is moderate. Baro-facilitation causes the blood pressure to fall. Obviously even high gains cannot force the pressure to drop below the baroreceptor threshold. The effect of the cardiopulmonary reflex on pressure and cardiac output is small at facilitation. At inhibition however, the cardio-pulmonary reflex reduces the pressure rise and enhances the cardiac output rise. An equivalent result is found by Walstra [16].

5.7 Variability analysis

In the previous chapter we found that baromodulation can explain the variability of arterial pressure that can be measured during 24 hour registration. Besides these variations another phenomenon that is measured is the periodic fluctuations. Closer investigation yields oscillation near 0.1 Hz in all pressure and heart rate signals. Therefore in this section we will look at the spectra of both blood pressure and heart rate.

Looking at spectra of blood pressure and heart rate registrations we can determine the different spectral components. An example of auto regressive spectra that can be obtained from normal blood pressure recordings is shown in figure 5.8.

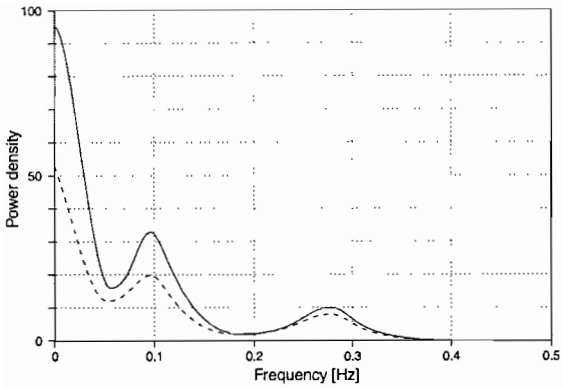

Figure 5.8 *Illustration of the blood pressure (solid) and heart rate (dashed) power spectral densities*

To derive the spectral density of the different frequency bands many different techniques are used. We will mention the standard method of measurement developed by the Task Force [14], a committee constituted by the European Society of Cardiology and the North American Society of Pacing and Electrophysiology. They distinguish three main spectral components in a short-term recording of 2 to 5 minutes: very low frequency (VLF), low frequency (LF) and high frequency (HF) components. In long term recordings an additional ultra low frequency (ULF) component is included. The frequency ranges are listed in table 5.8.

Table 5.8 *Frequency bands for heart rate and blood pressure spectra*

frequency band	Short term analysis	Long term analysis
ULF	-	≤ 0.003 Hz
VLF	≤ 0.04 Hz	0.003 - 0.04 Hz
LF	0.04 - 0.15 Hz	0.04 - 0.15 Hz
HF	0.15 - 0.4 Hz	0.15 - 0.4 Hz

In this thesis we will only discuss the short term analysis. In the HF band respiratory influences play a major role. In the LF band the 0.1 Hz rhythm explains the spectral density. The VLF and ULF bands refer to the slow drifts in the pressure and heart rate.

Looking at the variability, our model contains none of the above described variability. Pressure and heart rate are stable. This contradiction was examined in several studies. As a solution, investigators found that a resonance band near 0.1 Hz is present in the baroreflex system. However, at normal gains this resonance does not occur. Studies have proved that noise sources, present in the human body, activates the 0.1 Hz resonance which in its turn cause the 0.1 Hz variability.

Three different location have been identified:

- Peripheral resistance (spontaneous fluctuations)
- Baromodulation factor (sympathetic modulation)
- Baroreflex on heart rate modulation factor (vagal loop modulation)

For a detailed motivation for these choices we refer to the studies of Settels and Wesseling [17, 20, 21].

As low frequency variability is much stronger than high frequency variability (fig.5.8) we use one-over-f (1/f) random noise. In appendix B is described how we generated the noise. Because the noise is seen as a modulation it is applied as 10^x multiplier, with x a stochastic signal with a normal distribution and zero mean. The standard deviation defines the strength of the noise.

We have done some preliminary experiments with these noise sources in our model. The amplitude of the noise was defined in such a way that the spectra are similar to what was found in earlier studies[17, 20], listed in table 5.8.

Table 5.8 *Noise sources and their strength in the model*

Noise source	Noise amplitude [% RMS]
Peripheral resistance	3 %
Baromodulation factor	10 %
Baroreflex on heart rate modulation factor	10 %

The power spectra and coherence spectra are calculated as defined in appendix A. The results are showed in figure 5.9 to 5.12. What is clearly shown is that the ten second rhythm appears in all simulations. However the peak of this resonance band is not exactly located at 0.1 Hz but at approximately 0.08 Hz, the same frequency as found in the closed loop-gain (section 5.5). Stochastic peripheral resistance modulation causes both blood pressure and heart rate variability in the LF band of similar power. Coherence is high, especially for low frequency.

Stochastic baromodulation produces blood pressure spectra with a high density in the VLF band and almost no density in other frequency bands. In the heart rate spectrum both VLF and LF band have approximately the same densities. The coherence is rather high. Stochastic baromodulation primary causes slow blood pressure variability. This could be expected looking at the results of baromodulation and the 1.f properties of the noise.

The spectra of stochastic modulation in the baroreflex on heart rate show almost the opposite behavior. A very high density in the VLF band for heart rate. Some density in the LF band. The high influence on the heart rate spectra could be expected as the noise is present in this heart rate branch.

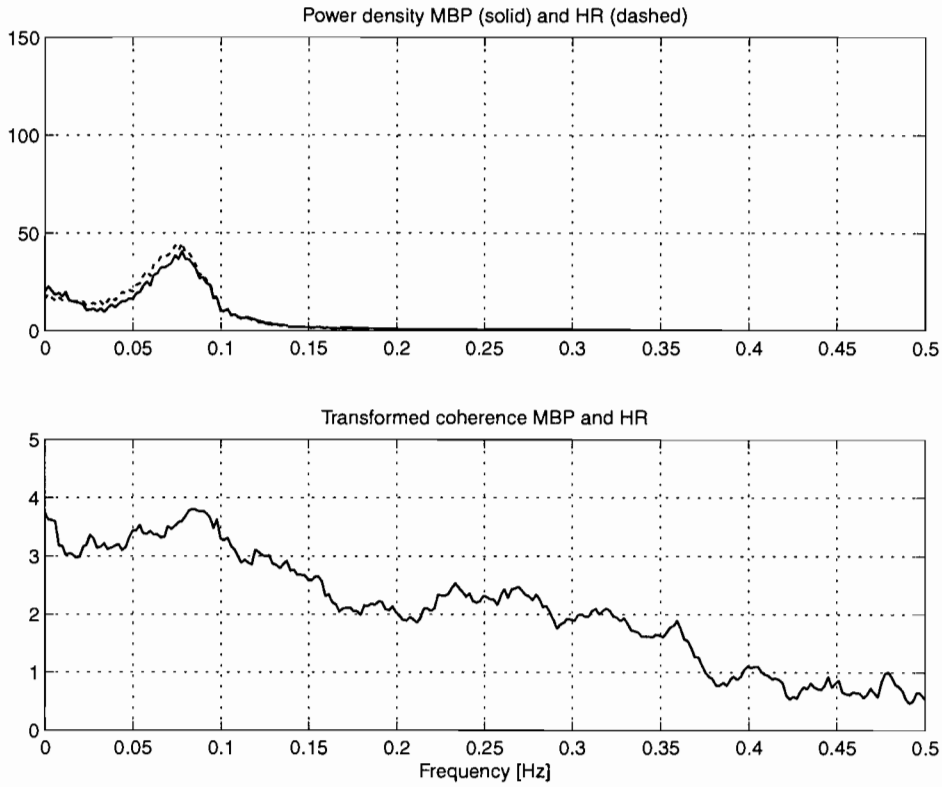

Figure 5.9 *Blood pressure and heart rate power spectra of the model with a stochastic peripheral resistance*

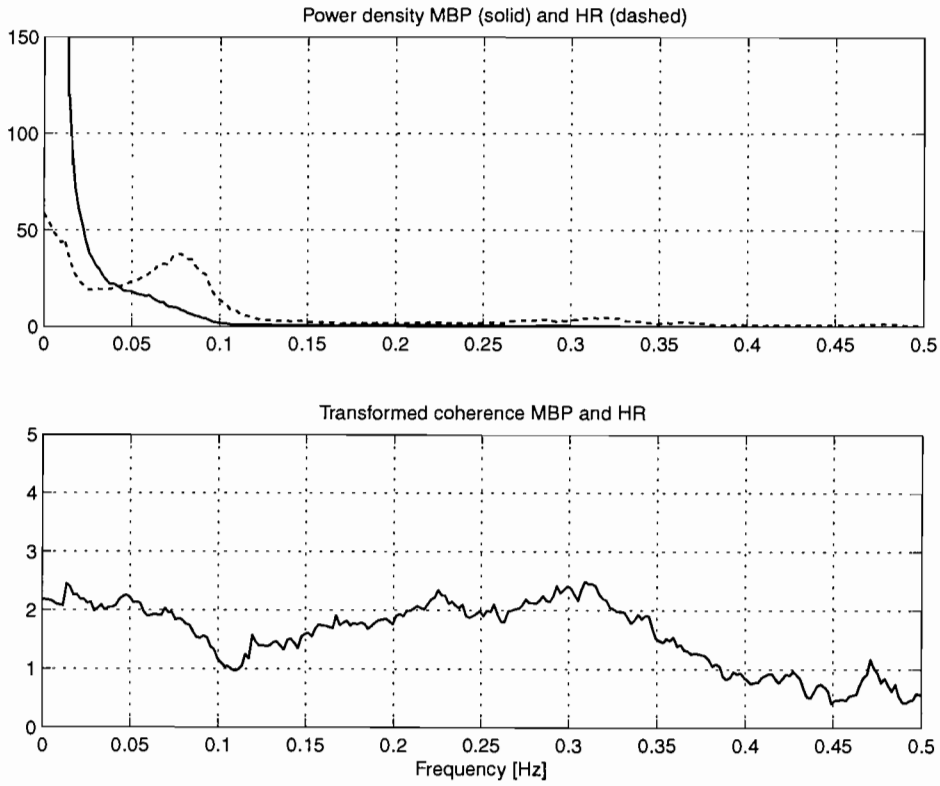

Figure 5.10 *Blood pressure and heart rate power spectra of the model with a stochastic baromodulation factor*

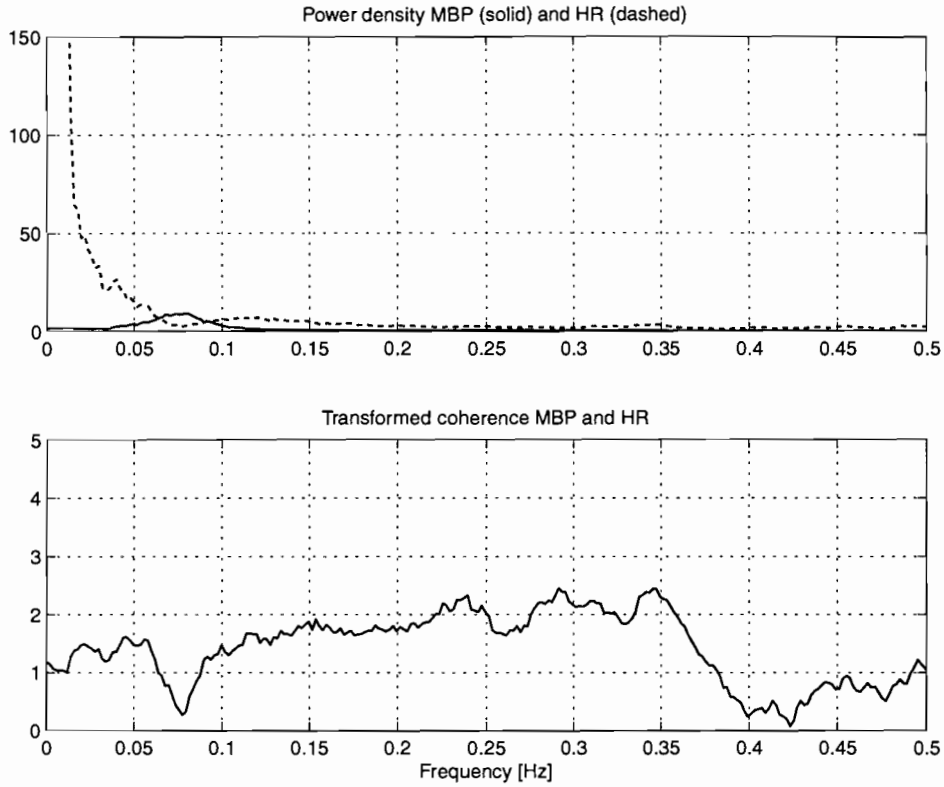

Figure 5.11 *Blood pressure and heart rate power spectra of the model with a stochastic vagal gain modulation factor*

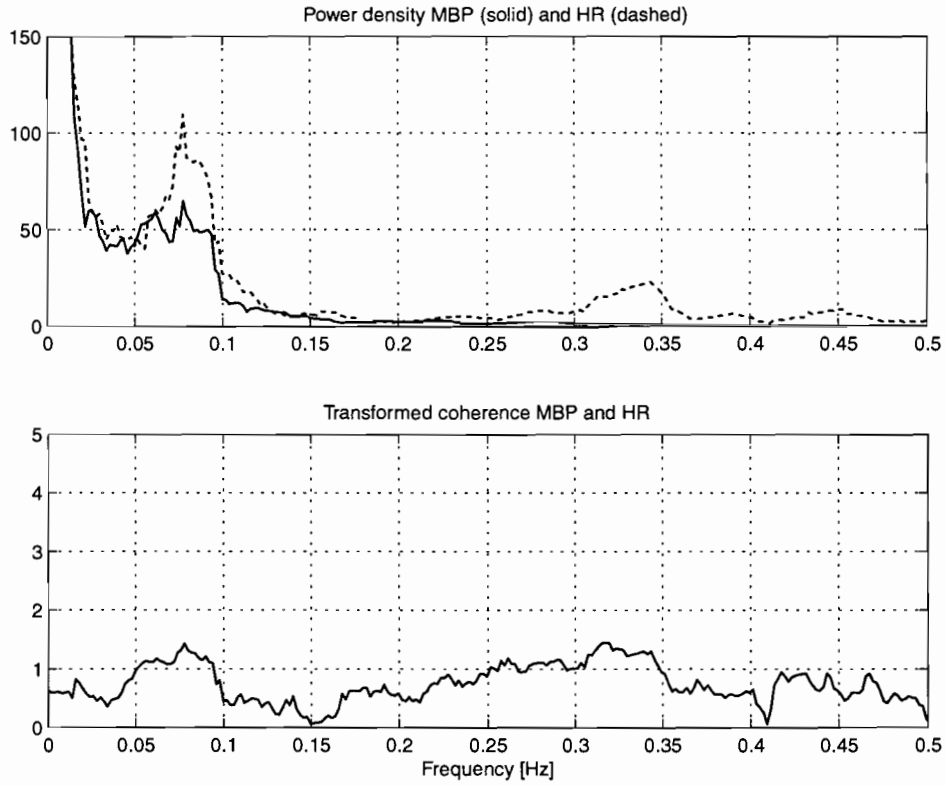

Figure 5.12 *Blood pressure and heart rate power spectra of the model with a stochastic peripheral resistance, stochastic baromodulation factor and stochastic vagal gain modulation factor*

If we turn on all noise sources simultaneously the model spectra begins to look like measured spectra. However their are still some aspects that cannot be explained yet, e.g. the steep slope at the right of the 0.1 Hz peak and the peak at approximately 0.3 Hz. The last appears to be the result of respiratory influences though respiration this is not simulated yet. So it is probably higher harmonics of lower frequencies.

Chapter 6 Conclusion and discussion

6.1 Conclusions

In chapter 2 we described the human circulation and its controls. Then we focused on the aspects that are important for the model requirements. We thereby emphasize that this description is incomplete. Next we divided the system in its two main parts, one, the circulation being the process of the system and two, the baroreflex as the regulating mechanisms.

The circulation was divided into sub-parts that were modeled separately. The hemodynamics differs for each part in detail. As general concept the windkessel model was adopted. For some parts like the aorta and the heart chambers the windkessel concept was extended with non-linear and time varying features. For the ventricles we used the varying elastance concept. In our simulations we have looked at the model in steady state. Mean pressures and volumes as well as their waveform agree with measurement results in humans. We concluded that the circulatory model reasonable mimics the human circulation.

The control model is based on an earlier developed model by Wesseling, Settels and Walstra[16]. In the heart rate control branch of the baroreflex we added a sympathetic stimulation of the heart rate. We studied step responses and open and closed loop gains. The result showed the different working ranges of the effectors. Fast mechanisms of vagal heart rate control showed small gains whereas slow mechanisms had a relatively larger gain. Hence the resulting system has a substantial gain over a wide frequency band. These results agree with measurements done in humans.

We also studied blood pressure and heart rate variability. Firstly we examined the effect of baromodulation. As proposed before, baromodulation may explain the sudden blood pressure rises that can be seen in blood pressure measurements. Baroreflex gain modulation is a sensitive way to change arterial blood pressure and cardiac output. The baromodulation curve of our model agrees with what was earlier found in other studies[16].

To explain blood pressure and heart rate variability spectra we added 1/f noise sources in our model. The spectra generated in the model are similar to what was found in measurements in humans. But we have not done a detailed study to validate these spectra.

6.2 Discussion

Developing computer models is a time consuming and complex task, especially for a process of nature such as the human circulation. Since such models can never achieve full similarity with the real system. One has to weigh all aspects and keep all needed aspects in the model. And some aspects are insufficiently studied in the detail needed for modeling, and thus left out unavoidable.

In humans the situation is even more complicated as it is unethical to interrupt the process or open control loops. Nerve traffic is notoriously difficult to measure also. All these factors make together that technology cannot completely model all phenomena of the human circulation.

Many models have been developed in past decades of which this model is one. Most of these models are only beat-to-beat, whereas ours is a continuous model. This leads, of course, to greater complexity and a greater number of parameters. Since we only allowed parameters that are well understood and have been verified with measurements, in some cases we had to replace complexity with commonly accepted simplicity.

An advantage of our model is its environment, Simulink, which results in a structure, divided in subsystems, that can be explored by 'double-clicking'. This way adjustments, extensions are easily implemented. Simulation results can be exported to Matlab, a computing environment that facilitates further signal processing.

Most experiments we did in steady state, in some others we applied setpoint steps. Further experiments should include challenges to the patient such as Valsalva maneuver, mental tasks and responses to drugs. The main reason for this new model was the study and understanding of baroreflex sensitivity. We indeed created a model is suitable for baroreflex sensitivity investigations as the experiments showed.

References

[1] R.D. Bauer, and R. Busse; *The arterial System*; Springer-Verlag; (Erlangen 1978)

[2] J.E.W. Beneken, B. de Wit; *A physical approach to hemodynamic aspects of the human cardiovascular system*; Physical Bases of circulatory transport: Regulation and exchange, A.C. Guyton, E.B. Reeve; W.B. Saunders. pp. 1-45; (Philadelphia 1967)

[3] G.F. Franklin, J.D. Powell, Abbas Emami-Naeini; *Feedback control of dynamic systems*; Addison-Wesley Publishing Company; (Stanford 1994)

[4] A.C. Guyton; *Arterial Pressure and Hypertension*; W.B. Saunders Company; (Philadelphia 1980)

[5] G.J. Langewouters; *Visco-elasticity of the human aorta in vitro in relation to pressure and age*; thesis Free University Amsterdam; (Amsterdam 1982)

[6] M.N. Levy; *Nervous control of the heart*; Cardiovascular system dynamics, J. Baan, A. Noordergraaf, and J. Raines, eds.; MIT Press; pp. 365-370; (Cambridge 1978)

[7] A. Noordergraaf; *Circulatory system dynamics*; Academic Press; (Pennsylvenia 1978)

[8] A.M. van Roon; *Short-term cardiovascular effects of mental tasks*; thesis University of Groningen; (Groningen 1997)

[9] H. Senzaki, C.H.Chen, D.A.Kass; *Single-beat estimation of end-systolic pressure-volume relation in humans* ; Circulation; vol. 94; pp. 2497-506; (Baltimore 1996)

[10] J.J. Settels; *Blood pressure fluctuations and hypertension*; thesis University of Technology Eindhoven; (Eindhoven 1980)

[11] N. Stergiopulos, J.J. Meister, N. Westerhof; *Determinants of stroke volume and systolic and diastolic aortic pressure*; American journal of physiology; vol. 270; pp. H2050-9; (Amsterdam 1996)

[12] H.A.J. Struyker Boudier; *Regulatie van de bloeddruk*; Wetenschappelijke uitgeverij Bunge (Utrecht 1979)

[13] H. Suga, K. Sagawa, L. Demer; *Determinants of instantaneous pressure in canine left ventricle* ; Circulation Research, vol. 46 pp. 256-63, (1980)

[14] Task Force of the European Society of Cardiology and the North American Society of Pacing and Electrophysiology; *Heart rate variability*; Circulation; vol. 93; pp. 1043-56; (London 1996)

[15] B.J. ten Voorden; *Modeling the Baroreflex, a systems analysis approach*; thesis Free University Amsterdam; (Amsterdam 1992)

[16] H.G. Walstra; *Modelonderzoek aan de baroreflex bloeddrukregeling*; thesis University of Technology Eindhoven; (Eindhoven 1981)

[17] K.H. Wesseling, J.J. Settels, H.G. Walstra, H.J. van Esch, and J.J.H. Donders; *Baromodulation as the cause of short term blood pressure variability?*; Applications of Physics to Medicine and biology, G. Alberi, Z. Bajzer, and P. Baxa, eds; World Scientific, pp. 247-276; (Utrecht 1983)

[18] K.H. Wesseling; *Physics of the Cardiovascular System*; Medical Physics; (Utrecht 1980)

[19] K.H. Wesseling, J.R.C. Jansen, J.J. Settels, J.J. Schreuder; *Computation of aortic flow from pressure in humans using a nonlinear three-element model*; Journal of applied Physiology; vol. 74(5); pp. 2566-73; (Amsterdam 1993)

[20] K.H. Wesseling, J.J. Settels; *Baromodulation explains short-term blood pressure variability*; Psychophysiology of Cardiovascular Control, J.F. Orlebeke, G. Mulder, and L.J.P. van Doornen, eds.; Plenum Publishing Corporation; 1985: pp. 69-97 (Amsterdam 1985)

[21] K.H. Wesseling, J.J. Settels, W. Wieling, G.A. van Montfrans, and J.M. Karemaker; *The Baromodulation Hypothesis, Baroreflex Resetting and One-over-f Blood Pressure Spectra*; Computer Analysis of cardiovascular Signals, M. Di Rienzo, G. Mancia, G. Parati, A. Pedotti, and A. Zanchetti, eds.; IOS Press; pp. 105-118; (Amsterdam 1995)

[22] K.H. Wesseling, B. de Wit, J.A.P. Weber, and N. Ty Smith; *A Simple Device for the continuous Measurement of Cardiac Output*; Advances in Cardiovascular Physics, D.N. Ghista; Karger, Basel; vol. 5 (Part II): pp. 16-52; (Utrecht 1983)

Appendix A

Amplitude spectrum, power density spectrum and coherence spectrum

Equation A.1 shows the Fourier transform to calculate the continuous spectrum $F(\omega)$ of a function $f(t)$

$$F(\omega) = \int_{-\infty}^{\infty} f(t)\ e^{-j\omega t}\ dt \qquad (A.1)$$

This transform is used in algorithms to estimate the discrete Fourier transform (DFT) of sampled data. The Fast Fourier Transform (FFT) is an example of an efficient algorithm for evaluating a DFT. However, these algorithms assume input data sampled with a fixed sample rate, in our spectral computation we only have beat-to-beat data in compliance with physiologic experiments from so-called point processes. This means that every sample corresponds to a beat. Yet a beat can be of varying length and we have no equal time sampled data. Thus, we have to use a modified DFT algorithm. The following describes how this can be implemented.

We will estimate the discrete spectrum at fixed discrete frequencies. The following algorithm is used to obtain the complex spectrum $X(k\Delta f)$

$$X(k\Delta f) = \sum_{n=0}^{N-1} x_n\ e^{-j\,2\pi\,k\,\Delta f\,t_n} \qquad (A.2)$$

with:

$$0 \le k\Delta f \le \frac{(N-1)f_s}{N}$$

Here, x_n is the n-th sample of the data taken at time point t_n. As said we calculate the spectra at frequency at fixed frequency points, f_s is this sample frequency. For the beat-to-beat variables we took $f_s = 1$ Hz because in steady state condition heart rate differs not much from 1 Hz. Consequently our spectral density (Δf) was $\frac{1}{N}$ and the maximum frequency that could be obtained from the spectra was $\frac{N-1}{2}$.

The amplitude spectrum $D_x\ (k\ \Delta f)$ can be derived from the above described complex spectrum according to:

$$D_x\ (k\Delta f) = |\ X(k\Delta f)\ | = \sqrt{X_R^2(k\Delta f) + X_I^2(k\Delta f)} \qquad (A.3)$$

X_R and X_I represent the real and imaginary part of the complex spectrum X respectively.

The two-sided power spectral density spectrum can also derived from the complex spectrum according to:

$$D_{xx}(k\Delta f) = \frac{1}{N} \mid X(k\Delta f) \mid^2 = \frac{1}{N} \left(X_R^2(k\Delta f) + X_R^2(k\Delta f) \right) \qquad \textit{(A.4)}$$

where N is the record length.

As the standard deviation of these estimates are quite large, we used a smoothing algorithm, applying ensemble averaging using a window according to:

$$\overline{D_x}(k\Delta f) = \frac{1}{M+1} \sum_{i=-M/2}^{M/2} D_x([k+i]\Delta f) \cdot W(i) \qquad \textit{(A.5)}$$

where W(i) denotes the window function. We used a 20 point Hanning window.

For estimating the cross spectral density of two signals *x(t)* and *y(t)* we used the corresponding complex spectra *X(f)* and *Y(f)* according to:

$$D_{xy}(k\Delta f) = \frac{1}{N} X^*(k\Delta f)\ Y(k\Delta f) \qquad \textit{(A.6)}$$

where X^* is the complex conjugate of the spectrum X.

The coherence spectrum can be estimated from the PSD and CSD according to [10]

$$\gamma_{xy}(k\Delta f) = \frac{\mid D_{xy}(k\Delta f) \mid}{\sqrt{D_{xx}(k\Delta f)\ D_{yy}(k\Delta f)}} \qquad \textit{(A.7)}$$

Because $|D_{xy}(f)|^2 \le D_{xx}(f) \cdot D_{yy}(f)$ it follows that $0 \le \gamma_{xy}(f) \le 1$. The statistical accuracy is determined using the Fisher z-transformation. This transformed coherence $\omega(k\Delta f)$ is calculated according to:

$$\omega_{xy}(k\Delta f) = \frac{1}{2} \ln\left(\frac{1 + \gamma_{xy}(k\Delta f)}{1 - \gamma_{xy}(k\Delta f)} \right) = arctanh(\ \gamma_{xy}(k\Delta f)\ ) \qquad \textit{(A.8)}$$

When $\gamma_{xy}(f) = 0.7$, about half of the variance of y is associated with x. Therefore, a value of $\gamma_{xy}(f) > 0.7$ was considered to be significant and indicated coherence in this study.

Appendix B

Noise sources

The objective of implementing noise sources into the model is to generate three noise sources that are statistically independent. The corresponding spectrum must have decreasing power for increasing frequency. We will generate a one-over-f spectrum also referred to as pink noise. Because the noise sources are used for spectral analyses in a narrow frequency band (1 mHz to 1 Hz) we will generate pink noise that contains spectral power only aver this band. These noise sources are created according to [8]:

$$S_i(t) = \frac{\sum_{k=1}^{N} \frac{1}{\sqrt{f_i[k]}} \sin(2\pi f_i[k]t + \phi_i[k])}{\sqrt{\frac{1}{2}\sum_{k=1}^{N} \frac{1}{f_i[k]}}} \qquad \textit{(B.1)}$$

where i ranges from 1 to 3 and is an index for the noise source, N is the total number of sine functions included, and $\phi_i[k]$ is a random phase shift. The phase shift is chosen randomly for each frequency and source. The probability function is uniform from 0 to 2π. The mean of S_i is zero and the standard deviation is one. The frequencies $f_i[k]$ are chosen according to:

$$f_i[k] = k\Delta f + d_i \qquad \textit{(B.2)}$$

with Δf the frequency resolution and d_i a small shift from the basic frequencies. This shift is different for each noise source, making them independent and incoherent.

The spectra that are estimated using these noise sources must have a frequency resolution of 0.002 Hz. The maximum desired frequency in the spectra is 1 Hz. To obtain this, we chose the following parameters for generating the three noise sources:

Table B.1 *Parameters of the noise sources*

Source index (i)	distortion constant (d_i)	N	Δf
1	0	500	0.002
2	-0.001	500	0.002
3	0.001	500	0.002